RE-ORDER NO. 74-120

DEVELOPMENT OF IMPROVED AMORPHOUS MATERIALS FOR LASER SYSTEMS

prepared for

CALIFORNIA INSTITUTE OF TECHNOLOGY
JET PROPULSION LABORATORY

RECEIVED
DEC 10 1974
JPL TO OFFICE

"This work was performed for the Jet Propulsion Laboratory, California Institute of Technology sponsored by the National Aeronautics and Space Administration under Contract NAS7-100."

(NASA-CR-145616) DEVELOPMENT OF IMPROVED AMORPHOUS MATERIALS FOR LASER SYSTEMS Final Report (Owens-Illinois, Inc.) 78 p HC $5.00 CSCL 20E
N76-11074
Unclas
G3/36 02213

Task Order No. RD-151

Final Report

by

George F. Neilson and Michael C. Weinberg

November 27, 1974

Owens-Illinois, Inc.
P. O. Box 1035
Toledo, Ohio 43666

RECEIVED
NASA STI FACILITY
INPUT BRANCH

Contract #953846

TABLE OF CONTENTS

		Page
	Summary	1
I.	Introduction	3
II.	Economic Considerations	7
III.	Experimental Study of Crystallization Behavior	11
	A. Glass Preparation and Analysis	11
	B. Thermal Gradient Oven Heating and X-Ray Diffraction Analysis	15
	C. D.T.A., Liquidus Measurements, and Crystallization	18
	D. S Phase and Summary	20
IV.	Origin of Crystallization at Normal Cooling Rates	23
V.	Feasibility Evaluation of Outer Space Production	28
	A. Overview of Crystallization Calculation	28
	B. Homogeneous Nucleation Calculation	29
	C. Growth Rate and Crystallization Calculations	33
	D. Critical Cooling Rate Calculations	35
	E. Outer Space Cooling Ability	38
	F. Conclusion of Feasibility	39
VI.	Laser	42
	A. Neodymium Lasers	42
	B. Laser Gain	44
	C. Results	45
VII.	Future Studies	48
VIII.	Conclusions	52
	References	54
	Illustrations	55

LIST OF ILLUSTRATIONS

Figure		Page
3.1	X-Ray Diffraction Pattern of Surface Crystals (S Phase)	55
3.2	X-Ray Diffraction Pattern of 30% CaO Ground Class (Bulk)	56
3.3	X-Ray Diffraction Pattern of Crystals Formed in Gradient Oven Experiment at 626°C	57
3.4	X-Ray Diffraction of Crystals Formed in Gradient Oven Experiment at 895°C	58
3.5	D.T.A. Scans Heating and Cooling	59
3.6	D.T.A. Scan-Heating Rate 10°C/Min.	60
3.7	X-Ray Diffraction Patterns of Crystals Formed During Liquidus Determination - 1009°C	61
3.8	Crystal Phases Observed at Various Temperatures	62
4.1	Microphotograph of Bulk Crystallites	63
4.2	Surface Crystallites in Splat-Cooled Sample	63
4.3	SAXS Curve of Quenched 30% CaO Glass	64
5.1	Viscosity-Temperature Curves for 10% and 20% CaO Glasses	65
5.2	Calculated Nucleation Frequency vs. Temperature for $\Delta S_{fR} = 4$	66
5.3	Calculated Growth Rate vs. Temperature for $\Delta S_{fR} = 4$	67
5.4	Calculated Nucleation and Growth Rates vs. ΔS_{fR} at T^M	68
5.5	Calculated Crystallization Factor vs. ΔS_{fR} at T^M	69
5.6	Calculated Critical Cooling Rates vs. ΔS_{fR} at T^M	70
6.1	Energy Level Diagram for Nd^{+++} Levels Involved in Lasing Activity	42

LIST OF TABLES

Table		Page
III-2	Laser Glass Compositions	12
III-2	Elemental Analysis of Surface Crystals	13
III-3	Crystal Phases that Appear as a Function of Temperature	16,17
V-1	Variation of Temperature and Time at Maximum Crystallization Rate as a Function of Entropy of Fusion Parameter	37
VI-1	Absorption/Nd^{+++} for Several Glass Compositions	46

New Technology

No reportable items of new technology have been identified.

Abstract

Crystallization calculations were performed in order to determine the possibility of forming a particular type of laser glass with the avoidance of devitrification in an outer space laboratory. Although the laser glass in question readily crystallizes in an earth environment, it is demonstrated that under the homogeneous nucleating conditions obtainable in a zero gravity laboratory this laser glass may be easily quenched to a virtually crystal-free product. Furthermore, experimental evidence is provided that use of this material as a host in a neodymium glass laser would result in more than a 10% increase in efficiency when compared to laser glass rods of a similar composition currently commercially available.

A number of experimental studies are described which provide the input data needed for the crystal nucleation and growth studies and also lend experimental support to the conjecture that the laser glass material under investigation can be produced with the avoidance of devitrification in outer space but not on earth. In particular, differential thermal analysis, thermal gradient oven, x-ray diffraction, and liquidus determination experiments were carried out to determine the basics of the crystallization behavior of the glass, and small-angle x-ray scattering and splat-cooling experiments were performed in order to provide additional evidence for the feasibility of producing this laser glass material, crystal free, in an outer space environment.

Summary

The purpose of this six-month study was to consider the feasibility of producing improved laser glass material in an outer space laboratory. The unique advantage of outer space, particularly germane to this study, is the zero g condition or weightlessness. This condition may be exploited to melt and form glass in outer space without relying upon a container. Since the container walls and impurities introduced into the bulk of the glass from the container walls serve as heterogeneous crystal nucleation sites, the elimination of the container will greatly reduce the ability for crystal nuclei to form in the melt and thus deter the devitrification process.

A major portion of this study was devoted to classical homogeneous nucleation calculations and crystal growth calculations for a laser glass system, which are appropriate for the conditions of an outer space laboratory. We demonstrate that in the absence of heterogeneous nucleating sites our experimental laser glass material may be readily formed crystal free.

In addition a number of experiments were performed in order to obtain information essential for the above calculations and to provide further evidence for the feasibility of producing our experimental laser glass in outer space and demonstrate the impossibility of its crystal-free production on earth. In particular, thermal gradient oven experiments, D.T.A. (differential thermal analyses) studies, liquidus determination, and x-diffraction analyses were performed to elucidate the fundamental phase behavior of the laser glass system under investigation. Furthermore,

SAXS (small-angle x-ray scattering) data were collected to study the possible existence of a phase separation mechanism acting as a precursor to the nucleation of the crystal phases observed. No evidence of a liquid-liquid immiscibility was found for the glass prepared via the standard air-quench procedure. Also a splat-cooling experiment was carried out to observe the crystallization behavior exhibited by the laser glass under very rapid cooling rates. It was observed that although small surface crystallites did form, the interior of the sample was crystal free. This result serves to illustrate the point that earth fabrication of this material will always be marred by crystallization due to surface contact, regardless of the cooling rate. Yet, it also indicates that in principle one may produce, in bulk, this material crystal free. Of course, on earth it is not feasible to produce laser glass by a splat-cooling technique (even if surface crystals did not appear) since only thin samples may be prepared in this manner.

Finally, the economics associated with laser glass production was assessed. We illustrated how a small increase in laser efficiency could produce a sizeable cost reduction in the USA laser fusion program. Furthermore, the fabrication of more efficient glass lasers could open up new markets for this product hitherto untapped.

I. Introduction

The primary objective of this program is to examine the feasibility of producing improved and novel glassy materials for use in laser systems in an outer space laboratory. Our current investigations, summarized in this report, have been restricted to an investigation of glasses which would be used in the fabrication of laser rods. Since the ultimate goal of this program is the development of materials for use in commercial products, the touchstone for our initial studies rests upon a commercially available Owens-Illinois laser glass. The basic ideas which underlie this feasibility study may be described as follows. A particular type of high quality Owens-Illinois laser glass is difficult to prepare (and hence costly) because of its tendency towards devitrification (crystallization). Furthermore, it has been observed that the tendency towards devitrification increases as higher concentrations of CaO are included in the glass. On the other hand, laser glass containing large concentrations of CaO are extremely desirable since it has been observed in our laboratory that the laser efficiency increases with increasing CaO concentrations present in the glass. Our contention is simply that in an outer space laboratory one will be able to produce high efficiency laser glass containing large concentrations of CaO with the avoidance of the devitrification that would occur on earth. In order to appreciate the basis for such a claim, one must understand the factors that aid the rapid crystallization of the glass that takes place on earth. Since the laser glass has a very high melting point, the formation and melting of the glass is carried out in platinum crucibles. During the course of reaction, melting,

and cooling platinum impurities are introduced into the melt. Furthermore, impurities in the atmosphere, and the container walls themselves serve as impurity sites during the cooling of the melt. It is well known that nucleation of crystals is greatly enhanced by the presence of foreign substances in contact with the melt (heterogeneous nucleation). This phenomena is due to the fact that the surface-free energy for crystal nucleus formation is lowered when nucleation can take place on a foreign surface. In outer space, however, heterogeneous nucleation may be avoided since melting and cooling may be performed in the absence of a container because of the zero-gravity condition. Nucleation then can only occur homogeneously. As will be illustrated subsequently, however, the rate of homogeneous nucleation is very small, and hence the melt can be cooled sufficiently rapidly in outer space so that nucleation (and hence crystallization) is avoided.

In the following section a discussion will be presented of the economic advantages of being able to produce a high efficiency laser glass in outer space. Here we only briefly mention some of the important applications of glass laser rods. Of primary importance is the use of laser glass in the fabrication of neodymium-glass laser systems for the experimental nuclear fusion program. In a recent article appearing in Scientific American it was stated that, "At this writing neodymium-glass laser systems have been chosen by all but one of the major laser-fusion laboratories in various countries as the prime vehicle they will use to prove the scientific feasibility of laser fusion."[1] Another application for neodymium glass lasers is associated with their possible use as range finders for the military.

In this report we shall show the feasibility of producing laser glass in an outer space laboratory by demonstrating the following four points:

1) The experimental laser glass material can be produced in outer space with the avoidance of devitrification.
2) The experimental laser glass cannot be produced on earth.
3) The laser efficiency of a neodymium-glass laser produced from this material will be enhanced.
4) There are sound economic incentives for the outer space development of the experimental laser glass.

Section II contains a discussion of the economics and importance of the production of more efficient laser glass material.

In Section III a description is given of various experiments performed to determine the crystallization tendencies of the laser glass under earth crystallization conditions. In addition, a discussion is given concerning the conclusions that may be drawn from these studies.

Section IV contains a description of various earth experiments which provide evidence for the plausability of producing crystal-free experimental laser glass material in outer space.

In Section V the details of the crystal nucleation and growth calculations appropriate for outer space conditions are presented. Also a brief commentary upon the required cooling rates to avoid devitrification is given.

Section VI presents evidence for the superiority of our experimental laser glass material with respect to the expected lasing efficiency of neodymium-glass lasers constructed from such material.

Section VII contains suggestions for the directions that a continuation of this study would follow.

Section VIII presents a brief summary and statement of our conclusions.

II. Economic Considerations

In this section we illustrate that there exist strong economic incentives for the outer space production of laser glass. As we have suggested, in an outer space laboratory it will be possible to fabricate laser glass material with an enhanced efficiency. Since laser glass is quite expensive the benefits of producing a more efficient laser glass material are apparent. For any particular application a cost reduction would ensue from utilizing a more efficient laser glass since a smaller quantity of this material would be needed. Furthermore, the cost reductions would be even greater when this more efficient glassy material is utilized in a complex system such as the experimental laser fusion system being constructed at Lawrence Livermore Laboratory. For example, if a laser glass of 10% higher efficiency were employed, then one could reduce the number of amplifier stages by 10% and still get the same power output. Since the laser system costs 5 to 10 times the cost of the glass components, a 10% increase in efficiency will pay for 50 to 100% of the total cost of the laser glass in that system. Since Lawrence Livermore Laboratory is currently using Nd^{+3} glass laser rods in their current experiments, this is not a mere academic point.

An additional feature of the economic picture which indicates the significance of this product is the estimated growth in the total glass laser market (in which O-I is the dominant figure) shown below:

1974 - $\$3.0 \times 10^6$

1975 - $\$3.5 \times 10^6$

1976 - $\$4.0 \times 10^6$

1977 - $\$4.5 \times 10^6$

These figures are based upon the current uses of glass lasers, namely, as the source for heating and imploding the fuel pellet in fusion reactions and military range finders. The commercial feasibility of laser driven fusion power plants would be greatly enhanced by the introduction of a more efficient glass laser.

The laser efficiency is an important factor in the consideration of the feasibility of laser driven fusion reactions for a variety of reasons. First of all, the overall gain obtained from laser fusion (ratio of energy out to energy supplied) is a function of the various efficiencies which enter into the process. Hence, increasing laser efficiency (which is a very realistic prospect) would increase the overall efficiency of the fusion process and thus enhance the gain. Also a certain minimum amount of energy must be supplied to the fuel pellet from the laser in order to obtain ignition. This requirement calls for very large power outputs from the laser in very short pulses. Thus, if laser losses are reduced, by increasing laser efficiency, the severity of the power output requirements of the laser will be correspondingly reduced.

As we mentioned previously, the neodymium-doped glass laser seems to be the most promising candidate in the search for a power source in the laser-driven fusion program. Ruby lasers have very low efficiencies and may not be fabricated into large, high-optical quality pieces without extreme difficulty. CO_2 lasers are more efficient than the current Nd^{+3} doped glass lasers, but suffer from at least two drawbacks. First of all, the short pulse power output obtained from such lasers is small compared to that obtained from Nd^{+3} glass lasers. In addition, the 1.06 μm light of the neodymium laser seems to provide a more efficient heating of the

fuel than the longer wavelength (10.6 μm) light emitted by the CO_2 laser.

For range finder applications, increased efficiency would not only reduce the cost, but also the number of components since a smaller power supply is needed. This, of course, would reduce the weight of the device. More important, however, are thermal considerations. Current glass lasers tend to get too hot as a result of the high power required to operate them. Again, a lowering of the input power, would allow glass lasers to operate much cooler and thereby be more competitive with YAG and ruby lasers. A glass laser would use much simpler components, e.g., a $200 rotating mirror could replace a $2,000 Q-switch. Users would certainly be willing to pay a higher price for the glass laser in return for a total system cost reduction as well as a less complex and more flexible system.

Other future uses of glass lasers include conversion of uranium to plutonium by neutron absorption for use in nuclear fission. This is attractive from the point of view of using a laser system as a small, fail-safe, breeder reactor. Neutron absorption could also be used for the destruction of isotopes in radioactive wastes. Commercial feasibility of these potential applications would be markedly hastened by large increases in glass laser efficiency.

Finally, it should be mentioned that since laser glass sells for over $800/lb., the cost requirement of at least $160/lb. is easily met. Owens-Illinois' laser glass is so expensive because of the difficulties that arise in the preparation of this material. These laser glasses are quite prone to crystallization and are very corrosive to all known crucible materials, including pure platinum. Furthermore, less than one part per million of microscopic platinum inclusion makes the laser glass

unusable. Since in an outer space laboratory the melting and cooling of the laser glass will take place without the use of a container (making use of zero-gravity condition) no platinum impurities will be introduced. Hence, the overall cost of fabrication of laser glass material may be reduced by eliminating "rejects" due to platinum impurities (which would be included in earth fabrication) and which add to the ultimate sale price of the laser glass. In fact, we estimate that this cost saving could amount to roughly an additional $100/lb. over and above those previously mentioned.

It is extremely difficult to predict the size that the total laser glass market would reach if all of the above applications were fulfilled. However, our company experts feel that if glass lasers were utilized for all of the new applications mentioned, then the total market for laser glass could easily increase by a couple orders of magnitude. Conservatively, this would place the total laser glass market at about $\$10^8$/year.

Finally, some rough estimates were made for the power requirements needed to melt large samples of glass. For a 50-60 lb. melt, roughly 11 kilowatt-hrs. of energy would be required, operating under maximum operating conditions. For a 100 lb. melt roughly 13 kilowatt-hrs. would be needed.

III. Experimental Study of Crystallization Behavior

The laser glass systems with which we are dealing are quite prone to devitrification when moderate to high percentages of CaO are included in the glass composition. In order to predict whether or not this devitrification can be avoided under outer space conditions, it is essential to determine some basic facts concerning the crystallization behavior of such systems here on earth. Thus, in this section we present the results of several experiments which have provided us with this essential information. In particular we shall discuss the preparation and analysis of the glass samples, the x-ray diffraction measurements of the crystals which were formed, the results of heat treatments of the glassy material at various temperatures, D.T.A. (differential thermal analysis) studies, and a liquidus determination measurement. As we shall see subsequently the above-mentioned studies were of critical importance to our further investigations in that they provide crucial parameters for our calculations as well information regarding the nature of the crystallization behavior of the dominant crystal phases.

A. Glass Preparation and Analysis

Initially samples of three different glass compositions were prepared. The base composition of each glass was identical, but varying amounts of CaO were introduced in place of SiO_2 (see Table III-1). One 5" x 1" x 3/4" bar and two 2" diameter discs were cast for each of

Table III-1

Laser Glass Compositions

Mole %	Composition 20	Composition 25	Composition 30
SiO_2	49.67	44.70	39.74
CaO	19.87	24.84	29.80
Li_2O	27.32	27.32	27.32
Al_2O_3	2.48	2.48	2.48
Nd_2O_3	.50	.50	.50
CeO_2	.16	.16	.16

the above compositions. The glass was melted at 1454°C in a platinum crucible in an air atmosphere. All samples were annealed for 1/2 hour at a temperature of 454°C. An electric furnace was used for all melting and heat treatments performed.

Composition 20 is quite close in composition (approximately 20% CaO) to a commercial U-I laser glass. Compositions 25 and 30 contain higher mole percentages of CaO, and will be referred to as experimental laser glass material. Although the major effort in the study is devoted to an investigation of laser glass composition 30, a brief discussion will be presented of the properties of all compositions melted.

The 20% CaO composition samples were of good quality, having very low seed levels and cord free. In addition, there was no evidence of devitrification to the naked eye. However, a few small crystallites were observed when the samples were viewed under magnification with crossed polaroids. Inspection of composition 25 resulted in similar observations. In the case of the 30% CaO samples, however, both surface and bulk

devitrification were easily detected without magnification. Surface crystallization appeared in "islands" and numerous crystallites were observed in the interior of the samples.

An elemental analysis was performed via a microprobe technique, of the surface crystals appearing in the 30% CaO glass and those found in large chunks of 20% CaO laser glass previously prepared. The resulting chemical compositions are shown in Table III-2.

Table III-2

Elemental Analysis of Surface Crystals

Composition 20

	Glass wt. %	Crystals wt. %
SiO_2	55.65	∿ 70
Al_2O_3	4.72	∿ 4
CaO	20.78	∿ 6
Nd_2O_3	3.11	∿ .1
Li_2O	15.22	∿ 20
CeO_2	.52	-

Composition 30

No significant difference could be found between the chemical composition of the crystals and the glass.

One should note that the three important conclusions that may be drawn from the microprobe analysis are the following:

1) The surface crystals formed in the 20% CaO glass correspond to a lithium metasilicate based solid solution.

2) The chemical composition of the crystals from the 30% CaO sample is, within experimental error, the same as that of the glass.
3) The chemical composition of the crystals from the surface of the 30% CaO glass differs significantly from those taken from the 20% CaO sample.

In order to further analyze the crystal species formed, x-ray diffraction patterns were obtained from both crystal species. The crystals formed in glass composition 30 gave a sharp crystal pattern (see Fig. 3.1, 22 lines found), but could not be identified in terms of any crystal species containing the elements present. In the case of the crystals formed in the large chunk of glass of composition 20, 17 lines were found, and a generally good sharp pattern was obtained. Here, one phase could tentatively be identified as a solid solution having the base Li_2SiO_3 crystal structure (ASTM #15-519). The nine remaining lines could not be identifed with any known crystal structure having the elements present.

X-ray diffraction patterns were also obtained from the powdered glass (bulk) of the samples of the three compositions cast in this present study. All patterns appear quite similar and show no evidence of crystallinity (see Fig. 3.2 for diffraction pattern of composition 30).

The crystal species which form, in a given composition, is clearly dependent upon a large number of conditions. Time and temperature treatment, surface contaminants, and chemical composition no doubt play a large role in determining which crystal species are obtained. Furthermore, in light of the fact that crystal structures could not be found for several phases in both samples, one might suspect that metastable crystal phases are

being produced. In order to more fully understand the crystallization tendencies of our experimental laser glass, attention was restricted to one chemical composition (30% CaO glass) thus eliminating the complication of composition change upon crystallization. In addition, experiments were performed to elucidate the crystallization behavior of this composition under equilibrium conditions. These experiments will now be discussed.

B. Thermal Gradient Oven Heating and X-Ray Diffraction Analysis

A sample of 30% CaO glass, free of surface crystals, but containing a dilute concentration of small crystals in the interior, cut from a bar was placed in a thermal gradient oven with a temperature range from 482°C to 788°C for one hour. The sample was then removed from the oven and air quenched to room temperature. The portion of the sample that was heated above 595°C appeared as a chalky gray, opaque mass. The portion below 595°C appeared as a semi-translucent, smokey gray material. X-ray diffraction patterns were taken of four samples of material extracted from the bar. Two samples were on the high temperature side of the sharp dividing line at 595°C and roughly correspond to heat-treating temperatures of 626°C and 732°C. The other two patterns were taken of samples in the low temperature region and correspond to heat-treating temperatures of 518°C and 582°C. The two patterns taken from the low temperature end of the rod are quite similar, and show a number of relatively broad low intensity lines. Aside from a broad moderately intense line at d = 3.50 Å, the remainder of the spectrum may be identified as corresponding to some solid solution based upon a $LiAlO_2$ crystal phase (ASTM # 22-678). Furthermore from an inspection of the relative intensities and widths of the lines in these two spectrum, it is clear that the sample heat treated at the

higher of the two temperatures contains more crystalline material, which in some part at least is due to enhanced growth of the crystallites in the higher temperature region. The large breadth of the lines in both cases, however, indicate that the crystals are quite small. The spectrum obtained from the two samples on the high temperature end of the bar are quite complex, and in each case consists of a number of solid solution phases. The primary solid phases upon which the solid solutions are based have been identified, and are listed in Table III-3 below. The diffraction pattern of that glass heated at 626°C is shown in Fig. 3.3.

Table III-3

Crystal Phases that Appear as a Function of Temperature

Approximate Temperature of Sample	Phases	ASTM X-Ray Card File No.	Relative Amounts
518°C	Glass		Predominant Phase
and 582°c	$LiAlO_2$	22-678	Minor Phase
	Unexplained broad peak at 3.50 Å		
626°C	α'-$CaSiO_4$	20-237	Moderate Amount
	Li_2SiO_3	15-519	Moderate Amount
	$LiAlO_2$	22-678	Minor Phase
	$Ca_3Si_2O_7$	20-235	Trace Phase
	Perhaps some glass		(Minor Phase)
	Unexplained broad peak at 3.50 Å		

732°C	Li_2SiO_3	15-519	Moderate Amount
	$Ca_3Si_2O_7 \cdot 1/3H_2O$ or $Ca_3Si_2O_7$	11-316 20-235	Moderate Amount
	α'-Ca_2SiO_4	20-237	Minor Amount
	$LiAlO_2$	22-678	Minor Amount

The general features of the high temperature phases may be summarized as follows:

1) The intensity of the lines corresponding to the new phases (not found in patterns of glass held at 518°C and 582°C) is large and the lines are narrow indicating the existences of well developed and large crystals.
2) The $LiAlO_2$ phase is still present and the growth of this phase has been enhanced. This conclusion stems from the increase in intensity and narrowing of the $LiAlO_2$ lines found in the high-temperature heat-treated samples.

Since the results given above only pertain to a portion of the temperature region of interest, a second thermal gradient experiment was performed on a piece of 30% laser glass. The glass was placed in a platinum boat and inserted in a thermal gradient oven for 1/2 hour. The temperature range was 820°C-945°C. After the 1/2 hour heat treatment, the sample was removed from the oven and air quenched. Below 903°C a chalky gray-blue solid was observed. Above 903°C a white mass formed. Thus, one may conclude that the sample flows above this temperature. Since, however, in the temperature range from 903°C-945°C the sample was not clear, 903°C does not represent the liquidus temperature, but corresponds to the transition temperature between all solid phases and liquid + solid phases. The

sample was cut into several pieces and subjected to x-ray diffraction analysis. The three temperature ranges chosen were 825°C-830°C, 860°C-865°C and 895°C. The diffraction patterns obtained from these three samples are very similar, with that obtained for the 895°C glass shown in Fig. 3.3. It is clear that these patterns correspond to several phases. One minor phase has been identified as a lithium metasilicate phase which also appeared in the temperature range 626°-732°C. Also found was a minor amount of some unknown crystalline species (x phase) which could not be identified in the ASTM card file. However, by far the dominant phase observed in all 3 patterns is the phase denoted by S. This is a new phase which does not appear in the samples heat treated at lower temperatures. We shall subsequently discuss the prime importance of this phase to this present study. First, however, several other experiments performed will be briefly described.

C. D.T.A., Liquidus Measurements, and Crystallization

In order to find the glass transition temperature, T_g, and obtain information concerning the crystallization behavior of the 30% CaO sample, several D.T.A. runs were made (see Figs. 3.5 and 3.6). An initial rapid scan from room temperature to 1000°C was made heating at 10°C/min. and then a cool down of the sample at 40°C/min. Also two more detailed heat-up runs at 10°C/min. and 20°C/min. were made. The glass transition temperature could readily be identified in heat up and it was found that $T_g \approx$ 475°C at 20°C/min. Since the glass transition temperature is a function of heating (or cooling) rate, one would expect that the effective T_g for an air-quenched sample would occur at a somewhat higher temperature than the T_g values obtained with the above-mentioned heating rates.

T_g was not observed in cool down. This fact can be attributed to the intervening crystallization at some temperature higher than T_g. Exothermic peaks were found at 570°C and 638°C in heat up at a rate of 10°C/min. and at 585°C and 658°C at a rate of 20°C/min. These peaks correspond to the low temperature end of the crystallization of at least two distinct species. The 570°C and 585°C (and also 638°C and 658°C) peaks correspond to the same crystallization process and are merely shifted to a higher temperature at a more rapid cooling rate. The "equilibrium" lower limit to the crystallizations no doubt occur at somewhat lower temperatures. A more detailed analysis of the crystallization process may be made by a comparison of the D.T.A. traces with the results of the thermal gradient experiments. At both 518°C and 582°C the $LiAlO_2$ phase may crystallize from the melt. If one takes into account the time (and hence temperature) delay for crystallization due to the finite heating rate in a differential thermal analysis run, then the peak at 570°C (which would be shifted to lower temperatures as the heating rate decreases) could plausibly be identified with crystallization of this phase. The peak at 638°C may be identified with the crystallization of additional phases found in the higher temperature regime. The sharp endotherm which occurs at approximately 900°C signals the dissolution process which was observed at roughly 903°C in the high temperature thermal gradient experiment. In general, the D.T.A. results are supportive of the findings of the thermal gradient oven experiments. In addition, differential thermal analysis data has provided us with a reasonably good estimate of T_g.

The high temperature end of the region of interest is bounded by the liquidus temperature. In order to determine the liquidus temperature, small

samples of glass were heated in a platinum boat for 1/2 hour at a high temperature. Samples were then held at various lower temperatures for a long enough period to come to equilibrium at those temperatures. The samples were then air quenched. Those samples that remained clear and cooled to glass therefore must have been held at temperatures higher than the liquidus. Those samples which were held below the liquidus temperature appeared opaque when they were removed from the furnace and subsequently cooled to a crystalline mass. By means of this procedure, the liquidus temperature for the experimental laser glass was found to be 1010°C.

The crystals formed from those samples which were held just below the liquidus (972°C, 1002°C, and 1009°C) during the course of the liquidus determination were also subjected to x-ray diffraction analysis. The diffraction pattern of the glass held at 1009°C is presented in Fig. 3.7. This sample shows lines corresponding to solid solutions based upon several phases which have been identified. The three dominant phases are β-Ca_2SiO_4, Li_2SiO_3, and $8CaO \cdot 5SiO_2$ based phases. At 1002°C the β-Ca_2SiO_4 and Li_2SiO_3 based phases are also present, but the $8CaO \cdot 5SiO_2$ based phase appears to be absent. The pattern obtained from the sample held at 972°C is nearly identical to the one formed from 1002°C sample. It is important to note, however, that S phase does <u>not</u> appear in any of these traces.

D. S Phase and Summary

In view of the somewhat lengthy description of the experimental procedures and results presented, it may be of some benefit to briefly summarize the main conclusions that can be drawn from these studies. First of all, it is apparent that the crystallization behavior of the experimental laser glass system is quite complex. A multitude of crystal phases may

be formed, even under equilibrium conditions, as a function of temperature, as may be seen in Fig. 3.8. Furthermore, it was observed that crystallization proceeds quite rapidly with large growth rates very likely. Small samples will nearly totally devitrify if held below the liquidus for times of the order of a minute. The most significant result, however, is the appearance of the S phase in equilibrium crystallization experiments over a restricted temperature region. The primary aim of this current study is to determine whether crystallization of experimental laser glass may be avoided during the usual quenching procedure. As was mentioned previously, large surface crystals (as well as smaller crystals in the bulk) appear in our experimental laser glass subsequent to air quenching of the melt. The x-ray pattern of these surface crystals is shown in Fig. 3.1. One observes that the crystals formed may be identified as the S phase. Thus under the experimental conditions of interest, the most rapid crystallization taking place (and presumably the only process of significance) is that of S phase. This observation enormously simplifies the subsequent calculation of crystal nucleation and growth rates since we need only estimate the crystallization rate of the S phase. Furthermore, since we know the temperature range in which S phase tends to crystallize under equilibrium conditions, we also have an indication of the temperature range for which crystal nucleation and growth calculations must be performed. Although it is true that crystallization of secondary phases may play some role, this role will be of secondary importance compared to the nucleation and growth of S phase. If S phase crystallization may be avoided under outer space laboratory conditions, then it is quite reasonable to expect the total absence of crystallization since S phase crystallizes most rapidly.

In section V we demonstrate, via classical homogeneous nucleation and growth calculations, that indeed S phase crystallization in our 30% CaO laser glass may be avoided in an outer space laboratory.

IV. Origin of Crystallization at Normal Cooling Rates

When a commercial-type 20% CaO glass is prepared by cooling at normal cooling rates, bulk and surface crystallites of lithium metasilicate are sometimes formed, depending upon the method of melting. It is found that the concentration of these crystallites is dependent upon the amount of platinum introduced during melting. The nucleation of the Li_2SiO_3 crystallites may therefore be attributed to a heterogeneous mechanism with reasonable confidence under these conditions.

With our experimental 30% CaO glass it was indicated that the Li_2SiO_3 phase also appears as a major equilibrium phase upon heating the glass in the temperature range from about 1000°C to the liquidus temperature. However, with normal cooling rates from the melt, i.e., after pouring the glass into a steel mold and air quenching, only crystallites of S phase are detected. The formation of S phase crystallites, which were always found to be present under these cooling conditions, occurs both within the bulk and at the surface of the glass. A photomicrograph of typical crystallites of S phase found within the interior of the glass is shown in Fig. 4.1.

Since crystallites of only S phase, and not Li_2SiO_3, form in our experimental composition during normal cooling with the given method of preparation, it is assumed that the prevention of S phase crystallization will be of major concern during space fabrication of this laser glass. That is, since S phase is the only crystalline species found to form from the melt under normal rapid quench conditions, it may be assumed that it is the most probable phase to nucleate homogeneously under these conditions. It appears probable that crystallization of the Li_2SiO_3 phase,

of secondary concern, is initiated by a heterogeneous mechanism and can be prevented by containerless melting. We further assume that crystallites of S phase which appear to initiate at the glass surface are due to impurity particles which attach to the surface of the glass melt and which then serve as sites for heterogeneous nucleation, since there is substantial experimental evidence which indicates that the glass-air interface itself is not sufficiently favorable to allow for heterogeneous nucleation at the free surface.[2]

Since we were unable to prepare our experimental laser glass free of crystallites of S phase under normal, or production operation, melting and cooling rate conditions, we consider whether it is even possible to prepare a homogeneous glass under more favorable cooling rate conditions. To this end, the 30% CaO glass was melted and then rapidly cooled employing splat-cooling techniques by pressing a molten glob between copper blocks, thus obtaining a glass platelet nominally about 2 mm in thickness before the glass becomes rigid. Optical microscopic examination of these platelets were made for comparison with the micrographs of this glass prepared by the conventional cooling methods. In the splat-cooled samples, for which a micrograph is shown in Fig. 4.2, all crystallites appear to be in contact with the surface. No crystallites within the bulk of the splat-cooled glass were observed, in contrast to the conventionally cooled glass slabs where many crystallites were found interior to the surface. These results demonstrate that it should be possible to prepare a homogeneous glass under space conditions if the bulk crystallites do not form by a homogeneous mechanism. The experiments also show that with earth conditions, even under conditions of rapid quench, nucleation

and crystallization at a glass-melt interface cannot be prevented.

Conceivably, the bulk formation of S phase crystallites may occur through (1) a heterogeneous mechanism at the surface of foreign impurity particles such as platinum within the glass, (2) an inherently homogeneous nucleation mechanism, or (3) an initial amorphous phase separation followed by nucleation of S phase crystallites at the intersurfaces. This latter mechanism is believed to be involved in the formation process of certain glass-ceramic materials. In certain glass compositions under appropriate conditions, amorphous phase separation may occur by a spinodal mechanism which is characterized by the absence of an energy barrier for the initiation of the process. Thus, amorphous phase separation by spinodal decomposition may occur extremely rapidly and without an incubation period. If S phase crystallites form by the sequence of events of this last mechanism, there would accordingly be no way to prevent their occurrence under outer space conditions, other than by a change of composition to one lying outside of the immiscibility region.

Small-angle x-ray scattering measurements were thus made on a sample from a slab of the 30% CaO experimental glass which had undergone normal cooling, as well as on a sample of this glass which was further annealed at 500°C for 6 hours, to search for any evidence of amorphous phase separation. The scattering curves obtained for these two glasses were the same within experimental error and were of very low intensity. The scattering curve obtained for the annealed glass is shown in Fig. 4.3. Also shown in this figure for comparison are the scattering curves obtained under the same conditions for a homogeneous $MgO-Al_2O_3-SiO_2-ZrO_2$ CER-VIT™ type glass

™A registered trademark of Owens-Illinois, Inc.

prior to nucleation and for pure water-free fused silica. The CER-VIT glass contained a sufficiently small amount of nucleating agent (7, 8 weight percent of the ZrO_2) such that it was possible to quench it without the occurrence of appreciable phase separation of a ZrO_2-rich phase. It has been found that phase separation during quench in all-glass compositions which have been studied occurs on a sufficiently small scale (no greater than about 50 Å) such that it gives rise to an angular independent scattered intensity in the angle range depicted in Fig. 4.3. Thus in Fig. 4.3 only that scattering which occurs at angles greater than about 3 mrad can be attributed to scattering due to amorphous phase separation of the glass. It is noted that the scattering by the laser glass in this angular range is not much greater than that observed for a very homogeneous one component material (the fused silica), and is at least an order of magnitude less than that observed in glasses which have undergone appreciable phase separation. The upturn in the scattering intensity at scattering angles below 3 mrad is believed likely to be an artifact due to cracks in the glass surfaces, but this was not investigated further due to the preliminary nature of the investigation.

It was concluded from analysis of these SAXS data that no appreciable or measureable phase separation occurs in our experimental laser glass during quenching at the normal cooling rate. Also the SAXS data from the annealed glass show no evidence that spinodal decomposition may take place at th ese lower temperatures.

We thus conclude that amorphous phase separation is not involved in the nucleation of crystallites of S phase, which would therefore allow for the possibility of the fabrication of the homogeneous glass under

outer space conditions if homogeneous nucleation is not occurring. Indeed, the feasibility calculation presented in the following section does indicate that homogeneous nucleation is not involved in their formation. Also the experiments which have been described indicate that under earth conditions with conventional melting and cooling procedures, crystallization of this glass at the container walls cannot be avoided during cooling, and that bulk crystallization due to the presence of platinum particles may be impossible to prevent.

V. Feasibility Evaluation of Outer Space Production

A. Overview of Crystallization Calculation

In the previous section it was indicated that S phase is the only crystalline species observed to form in our experimental 30% CaO laser glass upon cooling from the melt. From the experiments carried out, it was also found that the chemical composition of S phase is very close to that of the base glass, and that S phase is the predominant crystalline species to form upon long-time heat treatments in the temperature range from about 800° to 900°C.

These results indicate that S phase will be the most probable crystalline species to nucleate homogeneously under normal cooling rate conditions since the crystallization of the other phases can be assumed to occur more slowly. Therefore, to determine if our experimental glass can be prepared homogeneously under outer space conditions, it appears that it is only necessary to calculate if the glass can be cooled from the molten state without the occurrence of appreciable homogeneous nucleation and growth of S phase. Stated otherwise, it appears adequate to determine by calculation whether homogeneous nucleation theory can account for the presence of S phase crystallites in the normally cooled experimental glass, since if this is not the case it may be assumed that a heterogeneous mechanism must be involved.

For the purpose of homogeneous nucleation calculations, it is fortuitous that S phase crystallizes with essentially no compositional change. In this case the crucial variables of classical nucleation theory, the bulk-free energy of crystallization of a nucleus and its

liquid-crystal surface tension, can be approximated with reasonable confidence from heat of fusion parameters, as will be shown. It will also be shown that the linear crystal growth of this nucleating phase can likewise be estimated from these same experimental parameters. All uncertainties in the values of the parameters and in the approximations made for calculating the nucleation and growth rates will be chosen as to indicate the largest probable overall crystallization rate as derived from them, that is for the worst possible case. For the determination from this crystallization rate of the total amount of crystallization upon cooling from the molten state, a procedure similar to that used for the construction of so-called time-temperature-transformation (T-T-T) curves will be employed. By this procedure a given volume fraction crystallized is selected, and the time required for this volume fraction to crystallize assuming continuous homogeneous nucleation is calculated at various temperatures over the temperature interval of concern. In our present calculation, after determining the nose of the T-T-T curve, which corresponds to the temperature where the crystallization rate is greatest, this maximum crystallization rate will be determined as a function of the heat of fusion parameter by a variational procedure. Finally, of estimate will be made from these results of the minimum cooling rates required to avoid various degrees of crystallization as a function of the heat of fusion parameter. These results will enable one to determine the longest cooling time which may be tolerated in order to limit the total fraction of crystallites to an acceptably low value.

B. Homogeneous Nucleation Calculation

According to classical homogeneous nucleation theory[2] for the

formation of crystalline spherical nuclei of the same composition as the matrix, the steady-state nucleation rate, I, may be expressed as[3]

$$I = (N_V^0 D/a_0^2) \exp(-\Delta G^*/kT) \tag{5.1}$$

where N_V^0 is the number of molecules per unit volume, a_0 is the molecular diameter, D is the kinetic coefficient for molecular transport across the nucleus-matrix interface, and ΔG^* is the free energy required to form a critical spherical nucleus given by

$$\Delta G^* = (16\pi/3)(\sigma^3/\Delta G_V^2) \tag{5.2}$$

In Eq. (5.2) σ is the liquid-crystal surface tension and ΔG_V is the bulk free energy change per unit volume for crystal formation. It has been shown that σ and ΔG_V may be approximated by the following[4,5]

$$\sigma = \beta \Delta H_f/(N^{1/3}V^{2/3}) \tag{5.3}$$

$$\Delta G_V = \Delta H_f T_R \Delta T_R/V \tag{5.4}$$

In Eq. (5.3), ΔH_f is the molar heat of fusion of the crystal at its melting point, N is Avogadro's number, V is the molar volume, and β is a constant which may range in value from about 0.33 to 0.5. In Eq. (5.4), T_R is the reduced temperature obtained by dividing the temperature by the equilibrium melting temperature, T_E, and $\Delta T_R \equiv 1 - T_R$.

If it is assumed that D in Eq. (5.1) may be equated to the liquid diffusivity as given by the Stokes-Einstein equation, then

$$D = kT/3\pi a_0 \eta(T) \tag{5.5}$$

where $\eta(T)$ is the viscosity. Employing Eqs. (5.1-5.5) and letting $\Delta S_{fR} = \Delta H_f/RT_E$ denote the entropy of fusion in units of R, one finds

$$I = \left[\frac{N_v^o kT}{3\pi a_o^3 \eta(T)} \right] \exp\left[+ \frac{16\pi\beta^3 \Delta S_{fR}}{3T_R^3 \Delta T_R^2} \right] \tag{5.6}$$

In order to evaluate Eq. (5.6), values for the parameters a_o, N_v^o, β, and ΔS_{fR} must be given. a_o was estimated from the size of the unit cell of S phase derived from x-ray data and was taken to be 5×10^{-8}cm. N_v^o is given approximately as 3×10^{22} molecules cm^{-3}. The value of I is relatively insensitive to these latter two parameters, and thus the precise values of a_o and N_v^o are not required. Since β can range from 0.33 to 0.5, for the present calculation a value of 1/3 was chosen to correspond to the most unfavorable case (of maximum nucleation rate). It has been found[5] that ΔS_{fR} associated with crystals that exhibit anisotropic and multifaceted growth satisfies the inequality $\Delta S_{fR} \gtrsim 4$. Since the S phase was observed to grow in such a fashion, the above condition appears appropriate for our calculation. Thus for the nucleation rate calculations a value of $\Delta S_{fR} = 4$ was chosen, since this value gives the highest nucleation rate at all temperatures. However, for the total crystallization rate calculations to be described subsequently, a range of ΔS_{fR} values from 4 to 20 were employed.

It may be seen in Eq. (5.6) that the viscosity as a function of temperature is also needed for the calculation of the homogeneous nucleation rate. Unfortunately, we were unable to obtain viscosity data on our experimental 30% CaO glass due to rapid devitrification of this glass in the temperature range of concern. However, the temperature dependence of viscosity was obtained on two similar glasses which contain 10% and 20% CaO. In Fig. (5.1) the solid line illustrates the temperature dependence of the viscosity for the 10% CaO glass and the dashed line for the 20% CaO glass. At

intermediate temperatures (750°C-950°C) the viscosities of the 10% and 20% CaO glasses are nearly identical. However, with decreasing temperature the viscosity of the 20% CaO glass may increase more rapidly than the 10% CaO glass. Since both the growth rate (as will be shown in the next section) and nucleation rates are roughly inversely proportional to the viscosity, it is evident that if there does occur an appreciable change of viscosity with increasing CaO content of the glass, it occurs in such a direction as to suppress crystallization in the higher percentage CaO composition glass. Extrapolating to 30% CaO, it is reasonable to expect this trend to continue. Therefore, we shall employ the viscosity data obtained for the 10% CaO laser glass in our present calculations with the expectation that these data will give a conservative lower limit to the suppression of nucleation and growth of crystallites from viscosity effects (that is, that these viscosity data, if in error, will be in that direction to predict a larger degree of crystallization).

Thus for interpolation of the viscosity data of the 10% CaO glass shown in Fig. (5.1) as is required for evaluation of Eq. (5.6), the empirical Fulcher equation was employed:

$$\log \eta(T) = A + B(T-T_0)^{-1} \tag{5.7}$$

In this equation T is the temperature and A, B, and T_0 are arbitrary constants. A least squares fit of the experimental viscosity data of the 10% CaO glass yield A = -1.3854, B = 2696.6, and T_0 = 561.88. Equation (5.7) with these values of the constants will also be employed subsequently to calculate the temperature dependence of the viscosity, knowledge of which is required for the determination of the maximum crystalliza-

tion rate of our 30% CaO glass.

The results of the nucleation calculation are shown in Fig. (5-2), where the log of the nucleation frequency is plotted as a function of temperature. In this figure the solid line illustrates the temperature dependence of the log of the pre-exponential factor. The decrease of this quantity at lower temperatures is caused primarily by the decrease of the viscosity in this range. The dashed line illustrates the temperature dependence of the exponential factor. The rapid increase of this quantity with decreasing temperature is due to a decrease in activation energy for critical nucleus formation at the lower temperatures. The sum of these gives the total nucleation rate and is illustrated by the dotted curve in Fig. (5.2). In the temperature range where S phase is observed to form (800°-900°C), it may be seen from Fig. (5.2) that the homogeneous nucleation rate may not exceed $10^{-22}cm^{-3}sec^{-1}$.

C. Growth Rate and Crystallization Calculations

A standard expression for the rate of advance of a crystal-liquid interface, per unit area of interface, may be written[6]

$$u = (fD'/a_o)\ [1 - \exp(-V\Delta G_v/RT)] \qquad (5.8)$$

Here u is the growth rate in cm/sec, f is the fraction of sites at the interface where atoms can be preferentially added or removed, D′ is the kinetic coefficient for transport across the crystal-liquid interface, a_o is the molecular diameter, V is the molar volume, and ΔG_v is the free energy change per unit volume accompanying crystallization.

In using Eq. (5.8), we assume that the kinetic transport coefficients for nucleation and growth rates are equal, and thus we employ Eq. (5.5) to evaluate D′ as a function of temperature.

Also Eq. (5.4) may be used to express G_v in terms of the undercooling ΔT_R. Thus, u is given by

$$u = [fkT/3\pi\, a_o^2\, \eta(T)]\, [1-\exp(-\Delta S_{FR}\Delta T_R/T_R] \qquad (5.9)$$

Since the growth rate increases with decreasing values of ΔS_{FR}, it is useful to determine the temperature dependence of crystal growth for the minimum value of ΔS_{FR}, $\Delta S_{FR} = 4$, as was employed for the nucleation calculation, and for f equal to its maximum value of unity at all temperatures, as this provides an upper limit for crystal growth rates. The Eq. (5.9) reduces to

$$u = [5.86 \times 10^{-3}\, T/\eta(T)]\, [1-\exp 4(1-1/T_R)] \qquad (5.10)$$

The resulting crystal growth rate as a function of undercooling was computed using Eq. (5.10) with the values of $\eta(T)$ as given by Eq. (5.7). The results are displayed in Fig. (5-3), where the solid line shows the temperature dependence of log u^3. The function u^3 is plotted, rather than u, since Iu^3 is proportional to the volume fraction of crystallites grown after a given time. As anticipated, this quantity is relatively large at high temperatures and falls off fairly rapidly in the low temperature region. The dashed line in this figure shows the variation of log I, as was plotted in Fig. (5-1). The sum of these two curves, or log Iu^3, is given by the long and short dashed curve. It should be noted that Iu^3 peaks at about 675°C. This temperature should correspond to the nose of a T-T-T plot, as will be discussed next.

If u and I are independent of time and if continuous nucleation and growth occur with increasing time, then the volume fraction of glass crystallized, X, in a time, t, is given by the Johnson-Mehl equation:

$$X = 1 - \exp[(-\pi/3)\ Iu^3\ t^4] \tag{5.11}$$

Since we are concerned with the formation of very small volume fractions of crystals, Eq. (5.11) can be approximated by

$$X = (\pi/3)\ I\ u^3\ t^4 \tag{5.12}$$

Thus Iu^3 is proportional to the volume fraction crystallized for small X, after a time, t, as was indicated. On a T-T-T (time-temperature-transformation) plot, a particular value of X is selected, and the times required for that volume fraction to form at various temperatures, corresponding to increasing amount of undercooling, may be calculated through the use of Eq. (5.12). The resultant time-undercooling curve exhibits a nose at some minimum time, due to the competition between driving force for nucleation and growth. This nose clearly occurs where, for some constant X, dt/dT = 0 in Eq. (5.12), and represents the temperature of maximum crystallization rate. From Eq. (5.12) one observes that the minimum in the t versus T curve (the nose) clearly corresponds to the maximum in the Iu^3 versus T curve already found. This maximum value of Iu^3 is also independent of the particular value of X, so the nose position on the T axis is independent of the value of X. The location of the nose of the T-T-T plot can therefore be determined, as required for the critical cooling rate calculations presented in the next section, by determining the maximum value of Iu^3 and the temperature at which it occurs, and then substituting the value of Iu^3 into Eq. (5.12) to determine the time required for the particular volume fraction chosen.

D. Critical Cooling Rate Calculations

The cooling rate required to avoid the crystallization of a given volume fraction of glass, $(dT/dt)_c$, may be estimated from Eq. (5.12) by means of the criterion given by Uhlmann,[6]

$$(dT/dt)_c = \Delta T^M/\tau_M \tag{5.13}$$

where τ_M is the time at the nose of the T-T-T curve, and $\Delta T^M = T_E - T^M$ the temperature at the nose of the T-T-T curve, is the undercooling. Equation (5.13) represents a more stringent condition than is required since with this cooling rate excessive crystallization is avoided even if crystallization occurs at all temperatures at the maximum rate. Thus Eq. (5.13) represents an upper limit to the cooling rate needed.

In our previous calculations of I and u, employing Eqs. (5.6) and (5.9), respectively, we let $\Delta S_{fR} = 4$. Also we set f = 1 at all temperatures in Eq. (5.9). These conditions may not be particularly appropriate for nucleation and growth of S phase, and in the following cooling rate calculations we attempt to choose more suitable and general criteria.

Uhlmann has indicated that for crystalline materials with large ΔS_{fR}, the condition $f = 0.2\ \Delta T_R$, where $\Delta T_R = 1 - T_R$, is a more suitable approximation for f. This refinement was included in our present calculations, and all of the following growth and crystallization results were obtained for $f = 0.2\ \Delta T_R$.

A further generalization of our calculation will be introduced by setting $\Delta S_{fR} = n$, with n an arbitrary integer equal to or greater than 4, so as to consider all entropies of fusion which may be appropriate to crystallites of S phase. Combining Eqs. (5.6), (5.7), and (5.9), with appropriate rearrangements of Eq (5.7), then yields an expression for Iu^3 in terms of only the parameters T_R and n. Then the value of T_R which maximizes Iu^3, denoted T_R^M, was found for arbitrary n by solving

$$\frac{d}{dT_R}\left[Iu^3\ (T_R, n)\right] = 0 \tag{5.14}$$

The preceding differentiation may be carried out in a straightforward manner. However, the resulting transcendental equation does not allow the explicit solution of T_R^M. Accordingly, a Fortran computer program was prepared to allow evaluation of T_R^M and hence ΔT_R^M for arbitrary n. This program was also used to compute $I(T_R^M, n)$, $u^3(T_R^M, n)$, $(\pi/3)\ Iu(T_R^M, n)$ from Eqs. (5.6) and (5.7), τ_M for given X from Eq. (5.12) and finally the critical cooling rate from Eq. (5.13).

The results illustrated in Table V-1 show how the values of T_R^M, ΔT_R^M and τ_M thus obtained vary as a function of the entropy of fusion parameter, n. $\Delta T_R'^M$ was calculated for T_E = 1283°K. The values of τ_M given were calculated for $X = 10^{-20}$. It is seen that the minimum time required to form even this extremely small volume fraction of crystallites at this greatest possible crystallization rate is always very long in terms of required cooling times.

Table V-1

Variation of temperature and time at maximum crystallization rate as a function of entropy of fusion parameters.

n	T_R^M	ΔT_R^M (°K)	τ_M for $X = 10^{-20}$ (sec.)
4	0.706	377	1.4×10^3
8	0.683	407	6.5×10^{11}
12	0.650	449	2.2×10^{20}
16	0.659	437	2.1×10^{28}
20	0.650	449	2.5×10^{36}

The results of the nucleation and growth r e calculations at the T_R^M corresponding to various values of n are illustrated in Fig. (5.4). In addition, the factor $(\pi/3)\ Iu^3$ for T_R^M is plotted as a function of n in Fig. (5.5). Finally we have calculated the necessary cooling rates as a function of the degree of crystallization at various values of n employing Eqs. (5.12), (5.13), and (5.14) and the results are shown in Fig. (5.6).

An inspection of Figs. (5.4) and (5.5) reveals that nucleation and growth rates are quite small and decrease as a function n at the respective T_R^M. It is clearly indicated in Fig. (5.6) that the required cooling rate to avoid crystallization of as little as one part in 10^{20} parts glass can easily be met.

E. Outer Space Cooling Ability

The heat loss, and hence the cooling rate, of hot glass on earth arises from both conduction losses to the container and radiation effects (the air convection heat losses are negligibly small). However, in a containerless outer space process, cooling is due solely to heat losses by radiation. Although this process will be more efficient than on earth, due to the lower black-body temperature of the surroundings, the overall cooling rate could be significantly lower under outer space conditions.

Order of magnitude calculations were made to determine the rate of heat loss in our glass employing classical black-body radiation theory. A number of complications arise in performing this calculation for glass because of its semi-transparent characteristics over the black-body frequency range in the temperature interval of concern. The radiation losses from opaque materials occur just from the surface and this loss can be calculated solely from a knowledge of the emissivity of the material in

conjunction with the Stefan-Boltzmann law. However, glass is found to be a bulk emitter over a portion of the frequency spectrum of concern and therefore one must know or be able to calculate its emissive power as a function of its thickness, in order to determine the heat loss as a function of time. Complications arise due to the internal emission, internal reflections, and absorptions, and remissions of radiation.

The estimates of minimum cooling rate obtained easily satisfy the requirements which were encountered in the previous section. However, due to the approximate nature of our calculation, we were unable to conclude whether the cooling rate in outer space will be faster or slower than on earth where both radiation and conduction losses are involved. If this becomes a sensitive matter, then more refined calculations can be made in the future.

F. Conclusion on Feasibility

In the preceding section we have considered in detail the factors which may lead to the homogeneous nucleation and crystallization of a phase of identical composition to that of the glass (S phase), under conditions which should be applicable for the containerless melting and cooling of outer space. It is our view that the ability to eliminate sites for heterogeneous nucleation via containerless melting is the most important of the several unique advantages offered by outer space fabrication. Nevertheless, the ability to fabricate our glass under conditions of high vacuum will insure the absence of any airborne impurity particles which may serve as surface sites for heterogeneous nucleation. We have no evidence that the conditions of zero or low gravity should have any appreciable effect on the tendency toward homogeneous nucleation, so long as the glass

composition does not fall in a region where liquid-liquid phase separation may occur, and provided that the glass can be prepared initially in a homogeneous condition. If the glass is initially unstable with respect to liquid-liquid separation, then the decrease in gravitational force would eliminate gravity induced convection effects, which in turn could conceivably retard the phase separation which is effective in initiating crystal nucleation. However, since no phase separation of our experimental laser glass was detected, such considerations were not explored.

Previously we calculated the required cooling rates to avoid the crystallization of various arbitrary volume fractions of crystals under homogeneous nucleating conditions. The greatest uncertainty in our calculations lies in our estimation of nucleation rates. Fortunately, the calculated critical cooling rate is relatively insensitive to error in nucleation rate because of the t^4 dependence in Eq. (5.12). From the data available we thus believe that our calculated cooling rates should be reliable to within about one order of magnitude.

It has been estimated that the avoidance of a volume fraction of 10^{-6} in the laser glass is required to maintain an acceptable product. However, for the least favorable entropy of fusion for crystallites of S phase ($n = 4$), we calculate that to obtain a glass containing no more than one part in 10^{20} of crystals, a cooling rate of only 0.25 deg K/sec. is required, as indicated in Fig. (5.6). From our radiant cooling rate calculations, we believe that this condition can easily be met. However, clearly, this crystallization level is many orders of magnitude smaller than required to form an acceptable product. It might be indicated that a volume fraction of 10^{-20} would result from a single crystallite about 1/4 μm in diameter per m^3 of

glass as the worst possible case. Thus at this crystal level, in the fabrication of a laser rod of less volume, there is a high probability that the glass will be totally crystal free. Even given the uncertainty estimated for the critical cooling rate values, the calculated results clearly show that the required minimum degree of crystallinity can readily be met, so long as we concern ourselves only with the formation of S phase by a homogeneous mechanism. We conclude that these calculations demonstrate the feasibility of preparing our experimental laser glass free of crystals under outer space conditions.

VI. Laser

A. Neodymium Lasers

Nd^{+++} doped solids have proven to be one of the most useful sources of laser materials. The neodymium laser is typical of a class of four level solid state lasers. Figure 6.1 is a schematic illustration of some of the processes that may occur in such a system. 0 denotes the

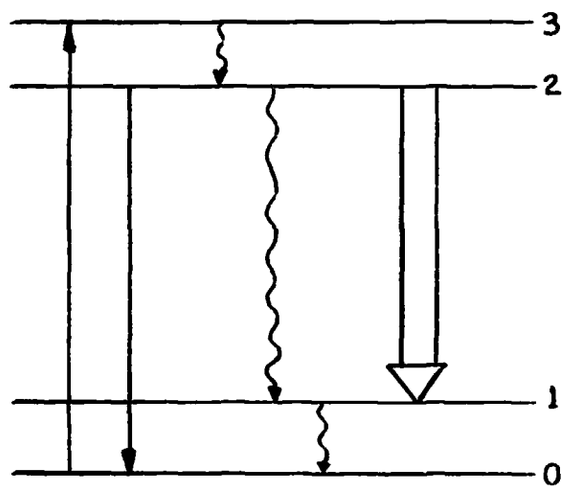

Figure 6.1

ground state and 1, 2, and 3 the relevant excited states for laser operation. The solid lines represent absorption or emission of light between the various levels indicated while the lines with wiggles represent non-radiative transitions. Typically light is absorbed from the ground state populating level 3. Level 3 is then depopulated by a rapid non-radiative transition to level 2. The lasing line is denoted by the broad arrow originating at level 2 and terminating at level 1. Level 2 may be depopulated by a variety of sources which include spontaneous emission to levels 0 and 1, non-radiative decay to level 1, and the

stimulated emission from level 2 to 1, which is the source of the laser output. Ions in level 1 must be capable of making a rapid transition by a non-radiative process to the ground state. Furthermore, at a specified operating temperature the 0-1 energy level separation must be sufficiently large so that the first level is not significantly thermally populated.

In the case of Nd^{+++}, the electronic structure of the ground state is such that three 4f electrons are populated in addition to the remaining closed shell structure. Within the Russel-Saunders coupling scheme it is observed that of the multitude of terms that may be constructed from three f electrons the ground state is given by $^4I_{9/2}$. The primary lasing transition in this system originates in the $^4F_{3/2} \rightarrow {}^4I_{11/2}$ transition. One should note that although $^4I_{11/2}$ does correspond to the first excited level of the system, the $^4F_{3/2}$ level lies above the second excited state. The energy difference between the states involved in the laser transition is about 1.06 μ. We also take note of the fact that all of the excited states pertinent to the lasing behavior of Nd^{+++} are formed from three 4f electrons. Hence, the lasing transition as well as all other radiative transitions of interest are symmetry forbidden transitions (4f $\rightarrow$ 4f type). Thus, we anticipate that the electric field produced by ions in the host lattice at the Nd^{+++} site will play a major role in determining the lasing behavior since such fields are capable of mixing states of different symmetry with the f orbitals (i.e., crystal field breaks symmetry).[9]

The host material for the Nd^{+++} may be either crystalline or glassy. If one uses a glassy host then the absorption and emission lines will be broad compared to that of a crystal host since each Nd^{+++} sees a somewhat

different environment in the glassy host. Glass lasers offer a number of distinct advantages which include the ability to readily vary the size and shape of the laser, ease in modification of the index of refraction of the host material, and the ability to produce high optical quality glasses.[10]

B. Laser Gain

The attenuation of light in an absorbant material follows the usual Beer's Law relationship

$$I_\nu(x) = I_0 e^{-k_\nu x} \tag{6.1}$$

where I_0 is the intensity of the incident beam, k_ν is the frequency dependent absorption coefficient and $I_\nu(x)$ is the intensity at a depth x in the material. It is also possible to express k_ν in terms of the parameters associated with the quantum mechanical transition[11]

$$k_\nu = \frac{\pi e^2}{mc} f_{ij} \left(N_i - \frac{g_i}{g_j} N_j\right) S(\nu) \tag{6.2}$$

where f_{ij} is the oscillator strength for the absorption from level i to level j, g_i and g_j are the degeneracies of the *ith* and *jth* levels; respectively, N_i and N_j are the number of atoms occupying the *ith* and *jth* levels, $S(\nu)$ is the line shape function, c is the speed of light, and m and e are, respectively the mass and charge of an electron. When the quantity $(N_i - \frac{g_i}{g_j} N_j)$ is negative, a population inversion of the states has occurred and k_ν is negative. A quantity α, called the gain coefficient, may be defined under these conditions as $\alpha = -k_\nu$. α is a measure of the enhancement of the light intensity in this population inverted system since $e^{\alpha L}$ (called the gain) determines the increase in intensity of the light traveling a distance L in the medium

via the Beer's Law equation. It is important to note that for situations where the population inversion is roughly constant, the gain coefficient is directly proportional to the oscillator strength (or the cross section for the transition).

We have mentioned previously that the nature of the laser glass host material could strongly influence the transition probability (i.e., cross section) of the Nd^{+++} lasing line. It has been observed that CaO is a particularly effective substance in enhancing this cross section: and, furthermore, it has been noted that the increase in cross section is roughly proportional to the increase in the mole % of CaO included in the glass. In turn, this enhancement of the cross section would yield a proportional increase in the gain coefficient. It has also been observed that if one pumps the laser with a short duration pulse (a case where one would expect the population inversion to remain roughly constant), then the overall lasing efficiency is roughly proportional to the transition probability for stimulated emission of the lasing line.

C. Results

The efficiency of our experimental laser glass material was compared to the efficiency of other laser glasses containing lower CaO content by finding the ratio of the cross sections for stimulated emission of the 1.06 μ line in the experimental glass to the others. This was accomplished by means of the following procedure. The relative absorption cross sections for the .88 μ line (ground state → initial state of lasing line) was measured for a number of laser glasses including our experimental laser glass. If it is assumed that the line shapes and branching ratios are identical in all glasses considered, then the ratio of the 1.06 μ cross section to the .88 μ cross section will

be the same for all glasses. This assumption is in accord with the observations made previously in our laboratory in this family of laser glasses. Listed below in Table VI-1 are the absorption coefficients for neodymium ion for the .88 μ line for two O-I laser glasses of lower CaO content and our experimental laser glass.

Table VI-1

Glass Composition	Absorption/Nd^{+++} $sec^{-1}cm^{-1}$
Experimental Laser Glass (30% CaO)	6.51×10^{-8}
O-I Laser Glass 1 (10% CaO)	5.49×10^{-8}
O-I Laser Glass 2 (20% CaO)	5.89×10^{-8}

On the basis of these experimental results, one expects our experimental laser glass to be 10% more efficient than the superior of the two O-I laser glasses listed above. An empirical correlation between glass composition and absorption of the .88 μ band has been formulated in the past for O-I laser glasses in this family of compositions. Use of this empirical equation for the absorption of our experimental glass predicts an absorption coefficient about 4% less than the measured value. This discrepancy could stem from an error in the chemical analysis for Nd^{+++} concentration or it could originate in the fact that for high CaO concentrations the cross section for absorption (and hence the overall laser efficiency) is higher than one would predict from empirical composition considerations.

Thus, in summary, we may state that there is evidence to lead one to believe that our experimental laser glass composition should be roughly 10% more efficient than the O-I laser glass with similar composition, but

20 mole% CaO content. This conclusion is based upon the measurements of the absorption at .88 μ in these glasses and our (O-I) experience and knowledge of such systems which allows one to draw the link between these measurements and the overall efficiency.

VII. Future Studies

Although a good deal of information pertaining to the crystallization tendency of our laser glass was ascertained during this study, and calculations presented have indicated the feasibility of avoiding devitrification of this glass in outer space, further experimental and theoretical work is clearly called for in order to bring this study to fruition. Thus, in this section we briefly indicate some future studies which we hope to initiate. These studies may be conveniently categorized into two areas: 1) melting and forming problems and 2) more detailed and expanded study of laser glass. Although both of the above-mentioned areas of endeavor are clearly relevant to this study, it should be recognized that a study of the melting and forming problems associated with laser glass fabrication in outer space is applicable to space glass and glass-ceramic formation in general.

A number of experiments have been planned in order to give additional confirmation of the results presented here, and to explore the opportunities for further extending the efficiency of our experimental laser glass. Since we have determined the temperature region in which the dominant S phase tends to crystallize from the melt, crystal growth rate experiments may be performed in this temperature region to obtain a more accurate measure of the growth rate of this dominant phase. Although the outer space nucleation rate will differ greatly from the "earth" nucleation rate, because of the homogeneous nucleating conditions in the former case, the outer space and earth crystal growth rates should be comparable. Also, the crystallization products should be studied as a function of cooling rate in order to evaluate the possible significance of crystallization of subsidiary phases. Another experimental test of our predictions may be made by the following. Laser

glass may be fabricated into many beads of small diameter. Those beads that are round to be virtually impurity free may be levitated and melted. The crystallization tendency of the levitated material may then be studied as a function of time and undercooling.

All of the experiments mentioned above would be aimed at providing experimental confirmation of the ability to produce our experimental laser glass in an outer space laboratory. However, additional earth experiments should be performed in order to test the ability to produce laser glass with even greater efficiency than our experimental laser glass. For example, melts could be prepared with percentages of CaO greater than 30%. Samples which do not completely devitrify would then be tested for their lasing efficiency. Similarly, compositions containing greater than 30% CaO could be experimentally studied in a fashion outlined in the previous paragraph. Furthermore, totally new glass compositions which promise to offer yet higher efficiencies, but cannot be formed readily in the bulk may be investigated.

It is anticipated that a major requirement that must be met by extended or new glass compositions which would permit the crystal-free formation of such glasses under the homogeneous nucleation conditions of outer space is that said compositions do not fall within equilibrium or metastable liquid-liquid immiscibility regions. Since phase separation in many cases tends to promote devitrification (even under homogeneous nucleating conditions), it is preferable to avoid the composition regions of the phase diagram where such liquid-liquid immiscibility may occur. Concurrent studies will be made to determine that this requirement is satisfied.

Several experiments are also planned to aid in the confirmation of the impossibility of fabricating our experimental laser glass on earth. As

was mentioned previously, both bulk impurities introduced from the platinum crucible as well as surface impurities introduced from the atmosphere and the container walls themselves serve as heterogeneous sites for nucleation. Melting and forming experiments in controlled atmospheres and with careful surface treatment of glass will be performed to test the effect on surface crystallization. Furthermore, attempts will be made to utilize crucibles free of platinum in order to study the bulk nucleation effects on earth. One should recall, however, that the laser glass material is quite corrosive so that one does not expect to easily obviate the bulk nucleation problem on earth by avoidance of platinum crucibles since there is a large probability that the molten glass will attack and partially dissolve any crucible employed.

The second major area of study will be concerned with glass preparation melting, and forming. Good laser glass must be homogeneous, and free of stria, bubbles and other glass defects. In outer space several problems will arise with regard to the production of defect-free glass. For example, on earth one possible mechanism for the elimination of gas bubbles in a glass melt is the loss of bubbles due to buoyancy effects. Bubbles having a large diameter will tend to rapidly rise out of the melt. However, in the absence of gravity such bubble rise will not occur. It is plausible to speculate that the bubble problem may be overcome by appropriate reaction techniques and the use of refining agents. Nevertheless, this problem deserves further detailed study. Also one must devise a method for appropriately reacting, melting, and "stirring" the reactants. Consideration must also be given to the elimination of the gas formed in the glass forming reaction and the appropriate control of such parameters as temperature, pressure, and gas

atmosphere. Although satisfying many of the above requirements will require thought and ingenuity, the current investigators will have at their disposal the years of accumulated experience and expertise which reside at Owens-Illinois in handling such special refining and forming problems. Furthermore, one of us is actively engaged in dealing with bubble melt defect problems, and thus may utilize this experience toward the solution of bubble defect removal in laser glass in outer space

VIII. Conclusions

In conclusion, we feel that we have demonstrated that there are strong incentives for a further investigation of this system. First of all, the economics of outer space laser glass production looks quite favorable. As we have indicated in Section II., not only is the market for glass lasers growing at a substantial rate, but we also anticipate an even more rapid growth if glass lasers with greater efficiencies are found. Furthermore, we have demonstrated that a relatively small increase in laser efficiency could produce quite impressive savings in the cost of complex systems such as those currently employed in the USA laser fusion program.

In addition, we have shown that production of our experimental laser glass will be feasible in an outer space laboratory, while there are strong indications that earth fabrication of this material will not be possible. These conclusions are based upon the observed earth crystallization of the experimental laser glass material abetted by the impurities of the container, and the calculations performed which illustrate the virtual absence of crystallization under the containerless melting conditions achieveable in outer space.

Finally, we have experimental evidence which indicates that our experimental laser glass material will have somewhat greater than 10% more efficiency than the current O-I laser glass material with similar composition but containing a 20% CaO content. It is important to note, however, that an even more substantial increase in the lasing efficiency may be gained by further increasing the CaO content of our experimental laser glass. In this current study our attention was limited to one com-

position due to time constraints as well to the realization that compositions containing very high CaO concentrations would devitrify to a much larger extent, making experimentation impractical. However, it is quite reasonable to expect, as suggested by our results, that the composition range, and hence efficiency, of our experimental laser glass may be increased by substantially more than 10% in an outer space laboratory.

References

1) J. L. Emmett, J. Nuckolls, and L. Wood, Scientific American 230 [6] (1974) 24.

2) D. Uhlmann, private communication.

3) J. H. Hollomon and D. Turnbull, Progress in Physics 4, (1953) 333.

4) D. Turnbull, Contemp. Phys. 10, (1969) 473.

5) D. Turnbull, J. Appl. Phys. 21, (1950) 1022.

6) D. R. Uhlmann, Materials Science Research, Vol. 4 (Plenum, N.Y.C., 1969).

7) D. R. Uhlmann, J. Non-Crystalline Solids 7, (1972) 337.

8) R. Gardon, J. Am. Ceram. Soc. 39, (1956) 278.

9) R. Gardon, J. Am. Ceram. Soc. 41, (1958) 200.

10) B. A. Lengyel, Introduction to Laser Physics (John Wiley and Sons Inc., N.Y.C., 1966).

11) E. Snitzer and C. G. Young, in Lasers, Vol. 2, Ed. Albert K. Levine (Marcel Dekker Inc., N.Y.C., 1968).

12) J. P. Gordon, in Laser Technology and Applications, Ed. Samuel L. Marshall (McGraw Hill, N.Y.C., 1968).

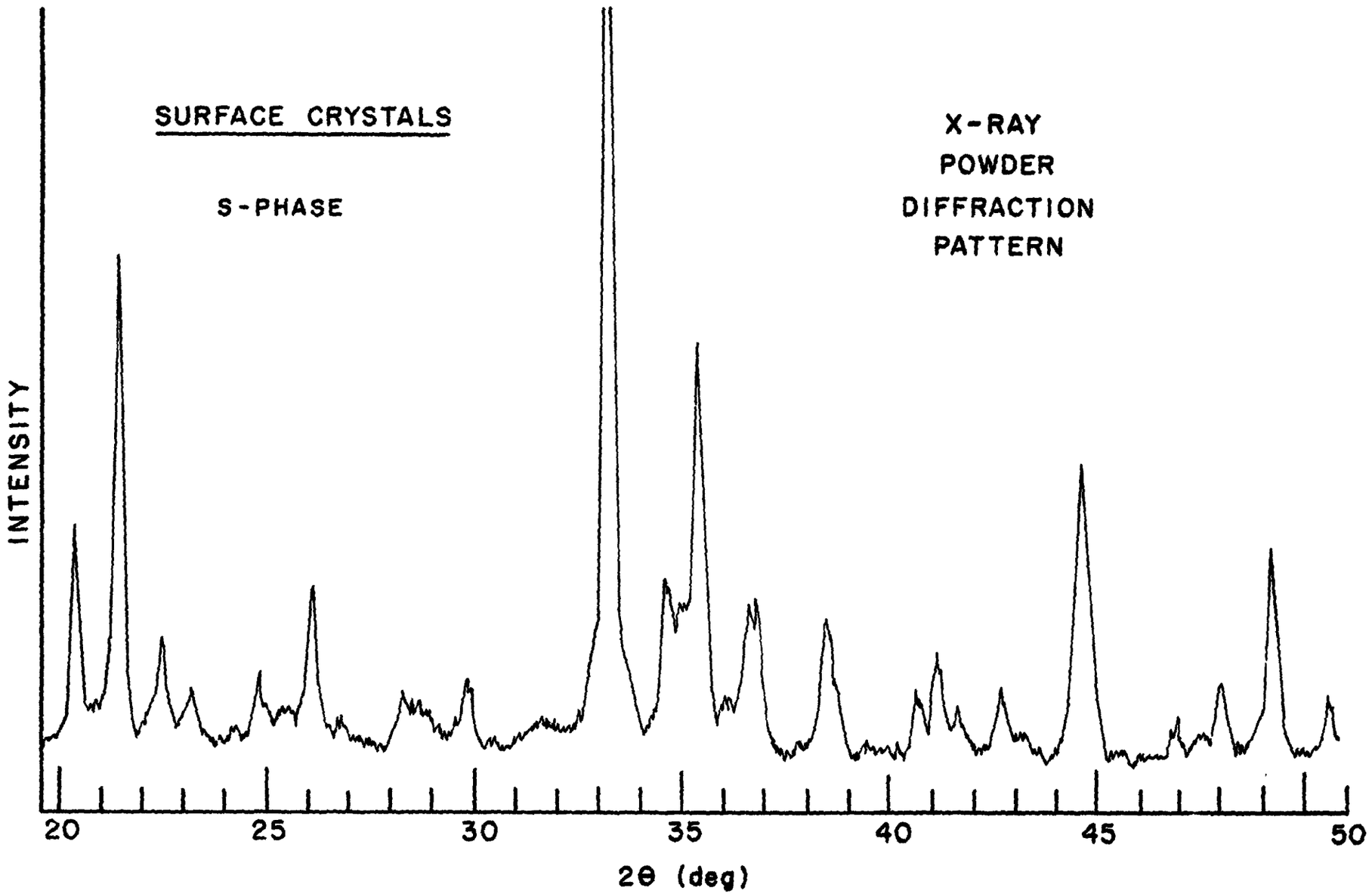

Figure 3.1

RO 24-120

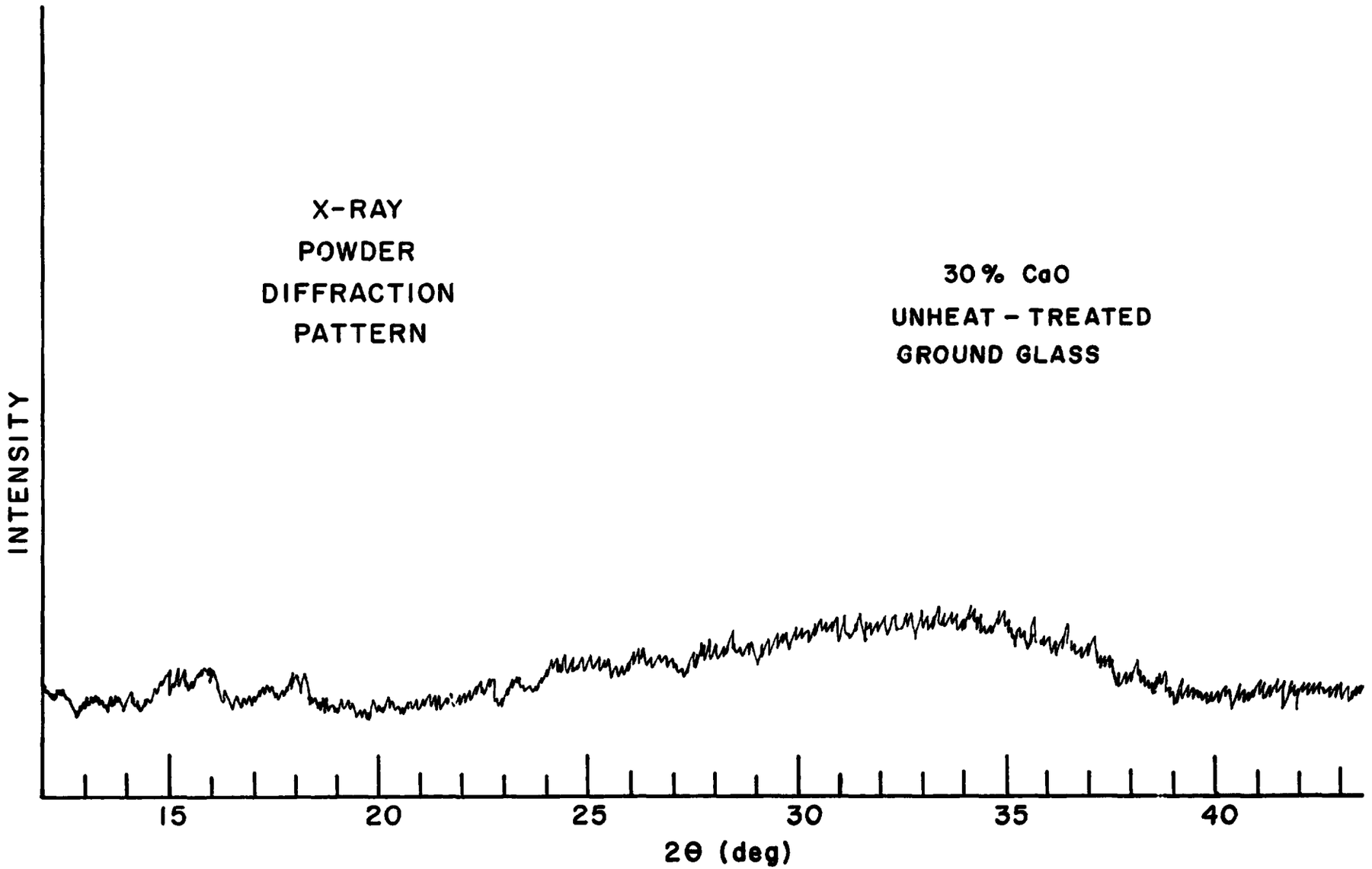

Figure 3.2

RO 71-120

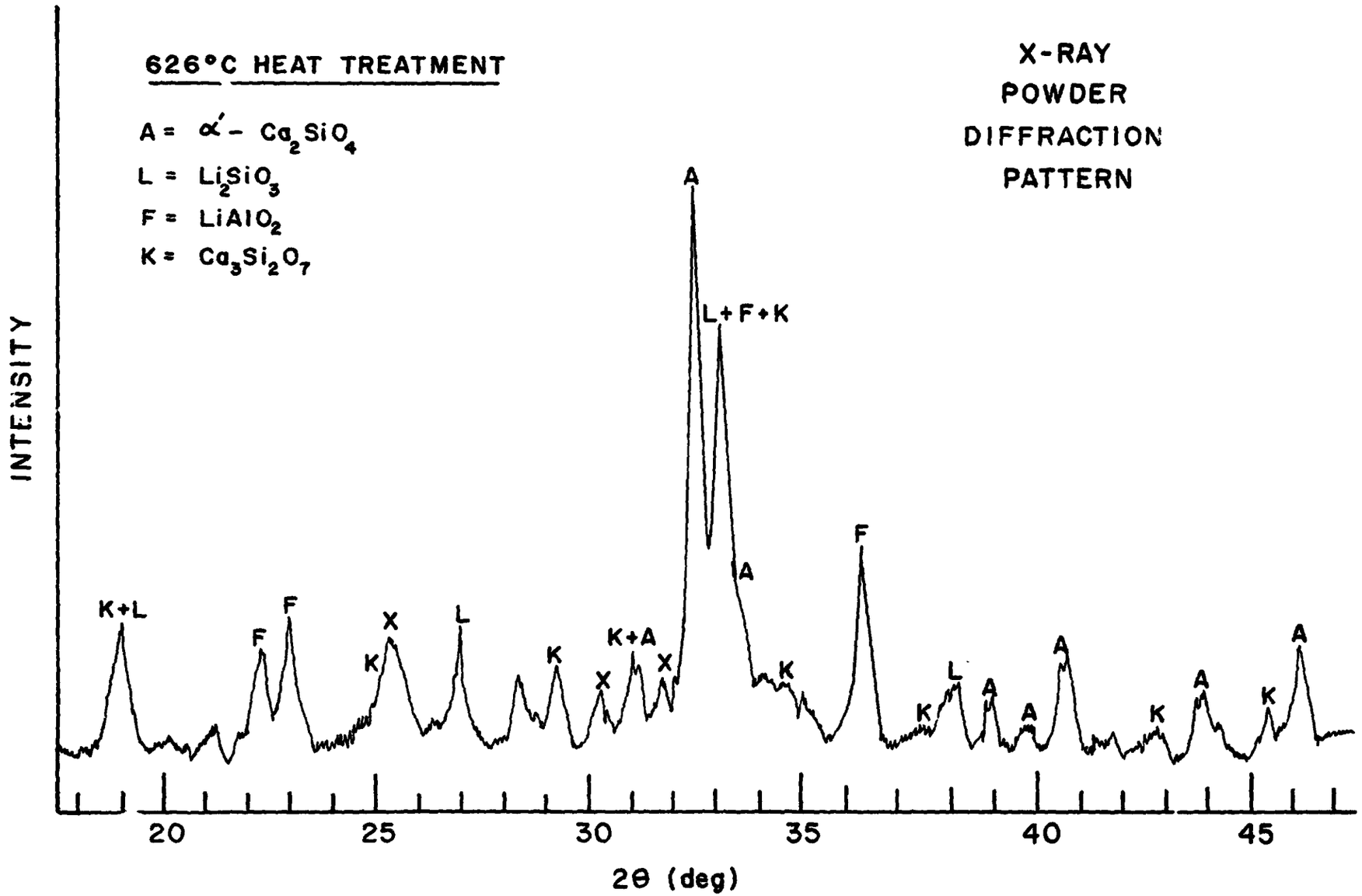
626°C HEAT TREATMENT
A = α′ - Ca_2SiO_4
L = Li_2SiO_3
F = $LiAlO_2$
K = $Ca_3Si_2O_7$
X-RAY POWDER DIFFRACTION PATTERN
INTENSITY
K+L
F
F
K
X
L
K
X
K+A
X
A
L+F+K
A
K
F
K
L
A
A
A
K
A
K
A
20
25
30
35
40
45
2θ (deg)

Figure 3.3

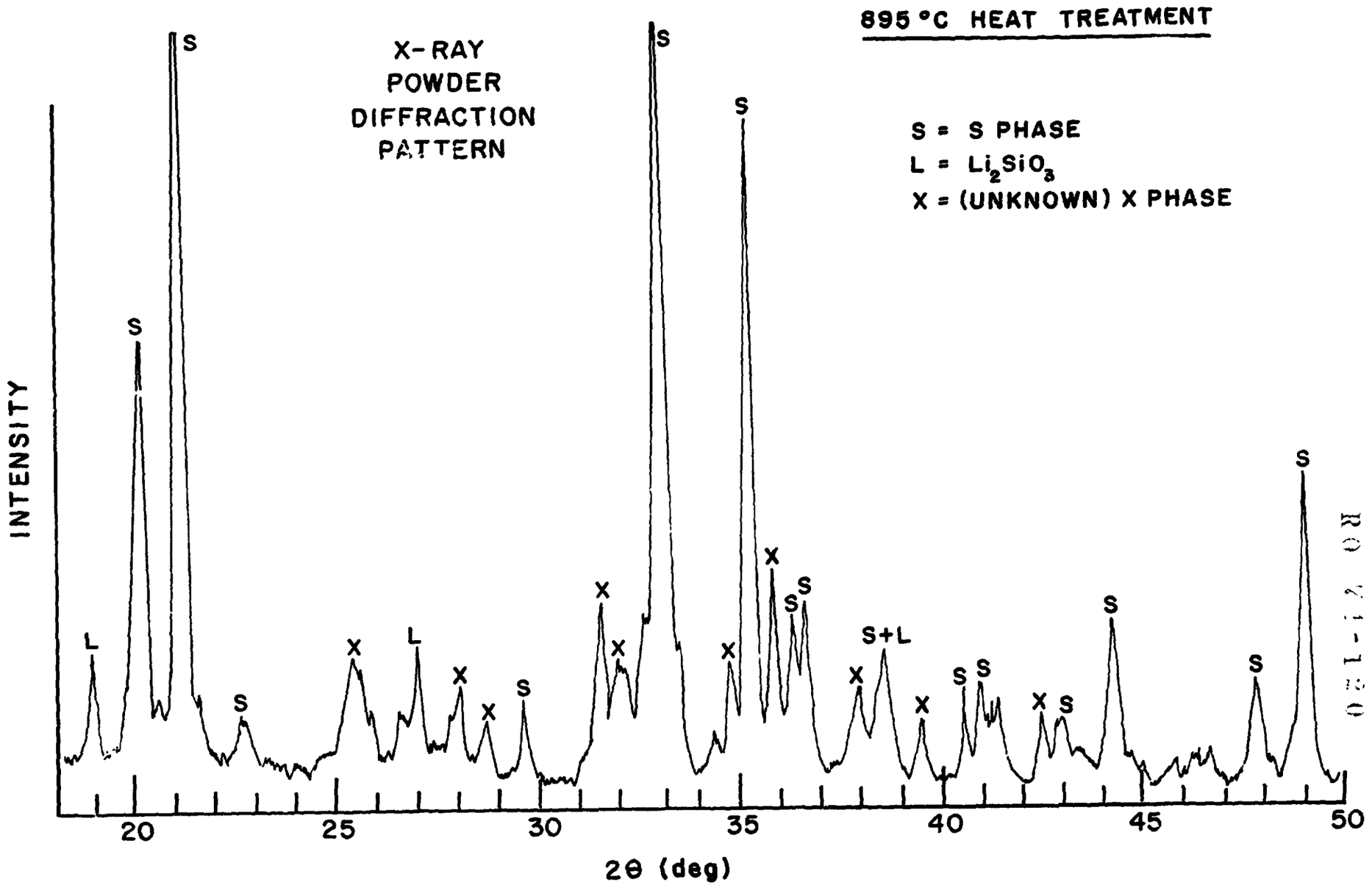
895 °C HEAT TREATMENT
X-RAY POWDER DIFFRACTION PATTERN
S = S PHASE
L = Li_2SiO_3
X = (UNKNOWN) X PHASE
INTENSITY
2θ (deg)
20
25
30
35
40
45
50
S
L
X
S+L

Figure 3.4

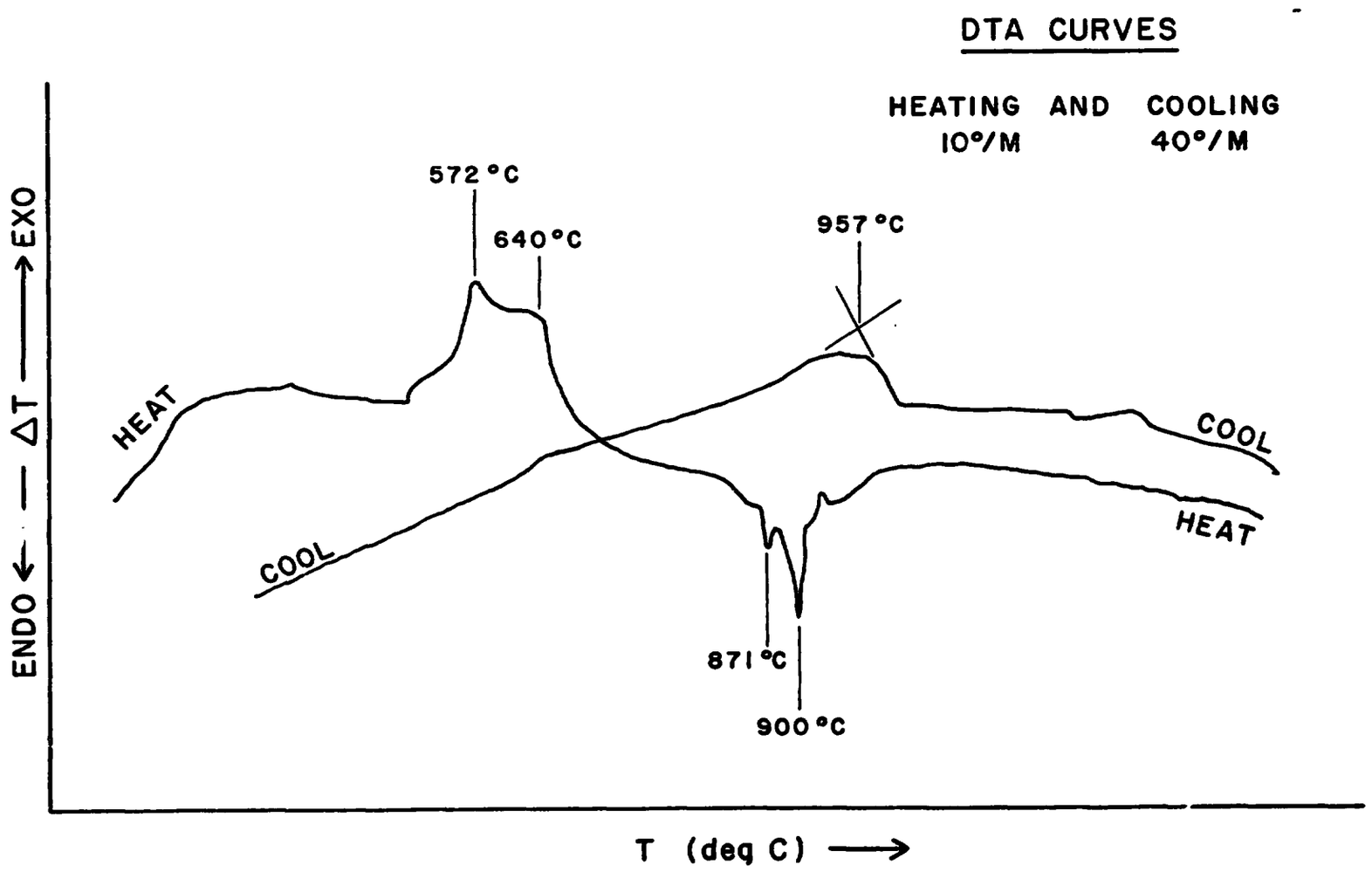

Figure 3.5

R0 [illegible]-120

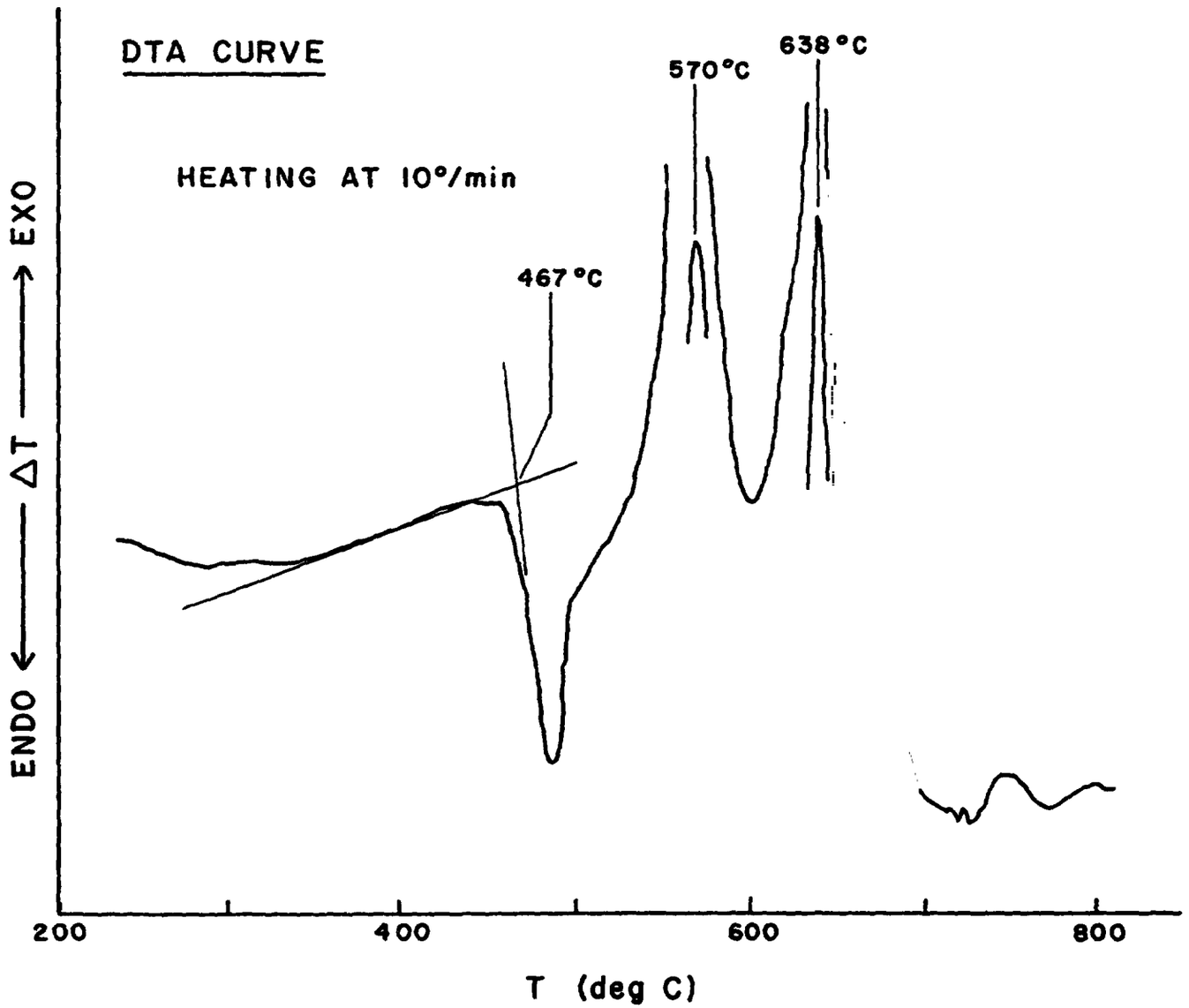
DTA CURVE
HEATING AT 10°/min
467 °C
570°C
638 °C
ENDO ← ΔT → EXO
200
400
600
800
T (deg C)

Figure 3.6

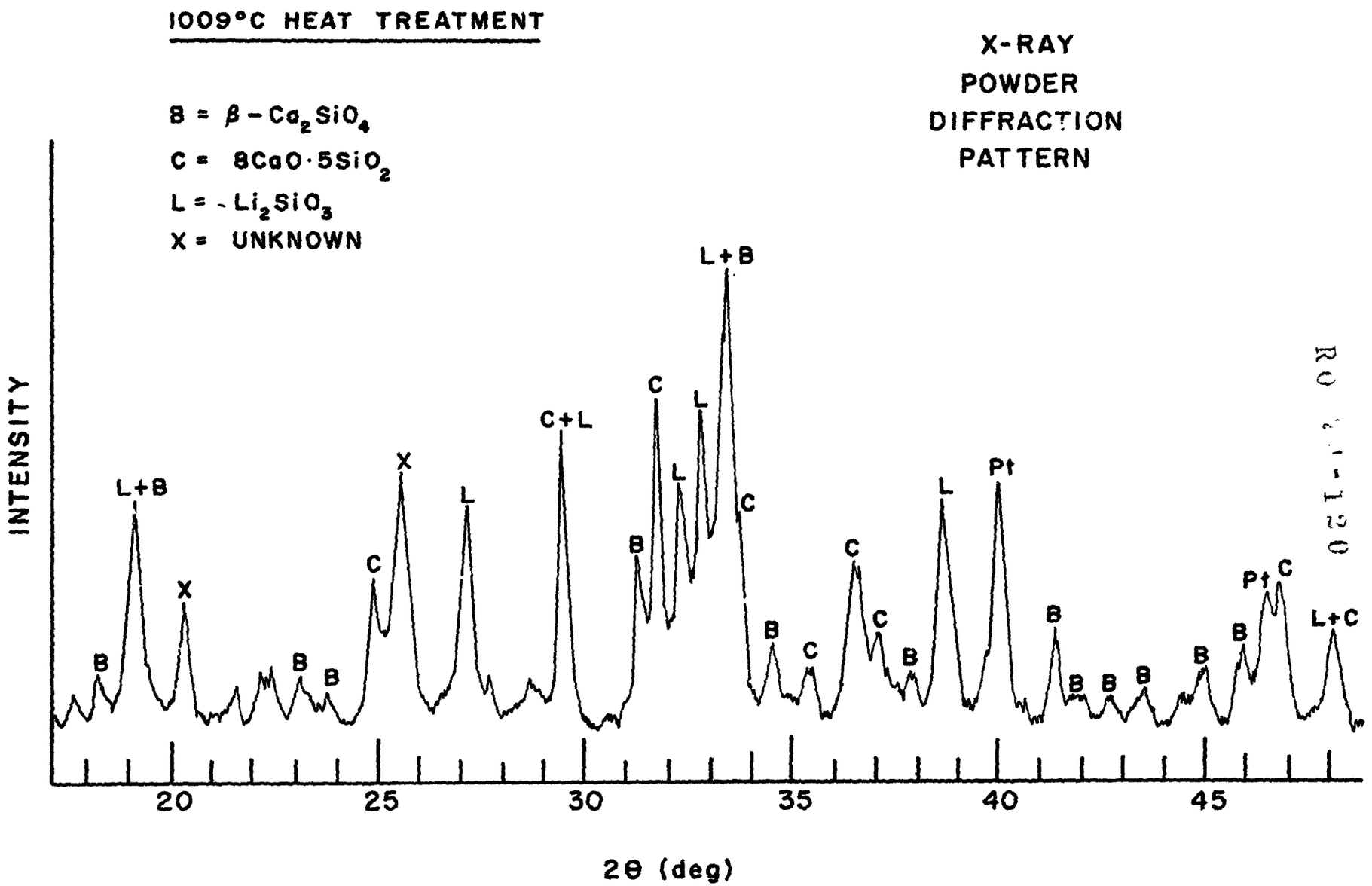
1009°C HEAT TREATMENT
B = β − Ca2SiO4
C = 8CaO·5SiO2
L = Li2SiO3
X = UNKNOWN
X-RAY
POWDER
DIFFRACTION
PATTERN
INTENSITY
2θ (deg)
20
25
30
35
40
45
L+B
X
B
C
L
C+L
Pt
L+C

Figure 3.7

Figure 3.8

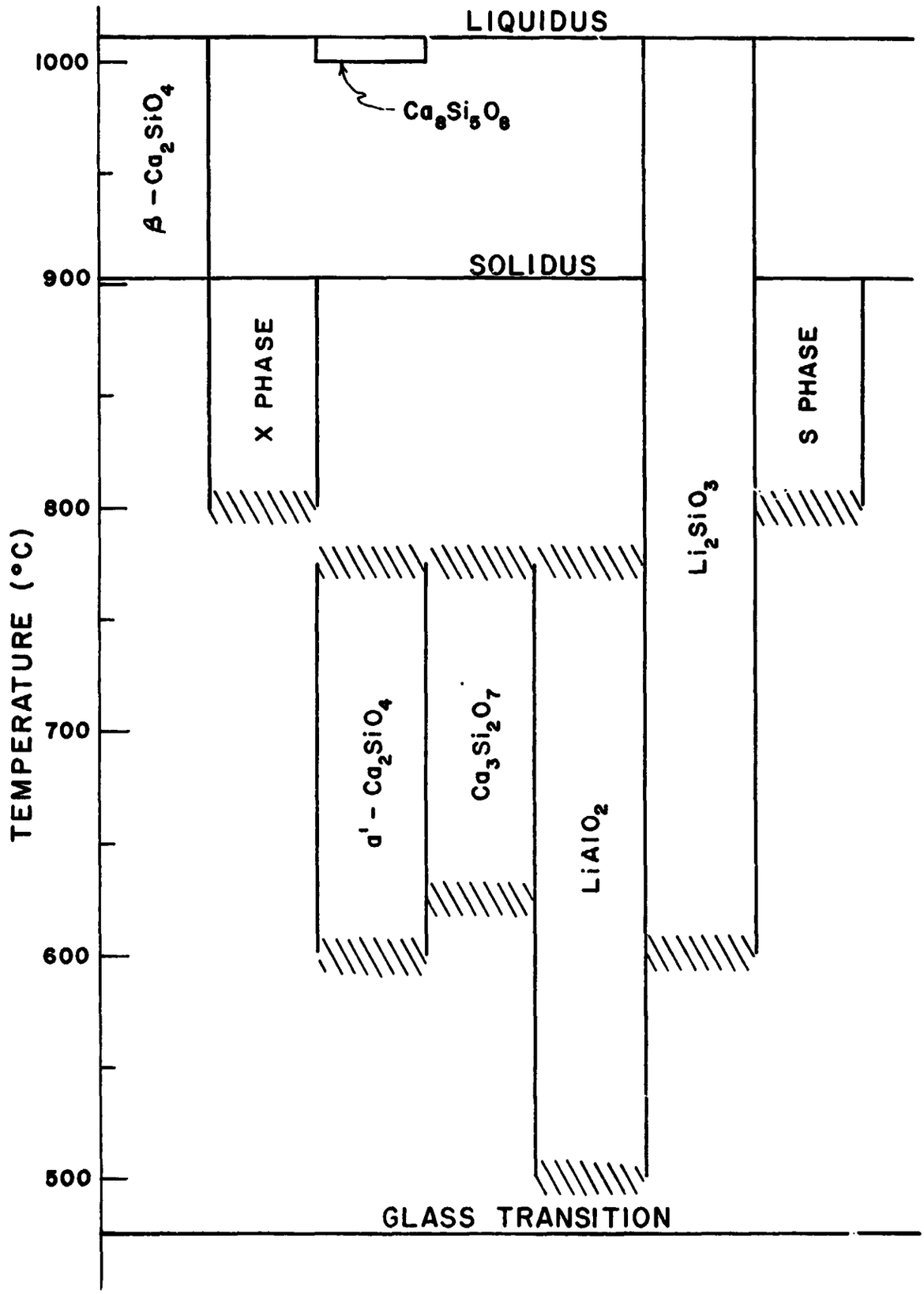
LIQUIDUS
1000
900
800
700
600
500
TEMPERATURE (°C)
β – Ca2SiO4
Ca8Si5O8
SOLIDUS
X PHASE
S PHASE
Li2SiO3
α' – Ca2SiO4
Ca3Si2O7
LiAlO2
GLASS TRANSITION

Microphotograph of Bulk Crystallites

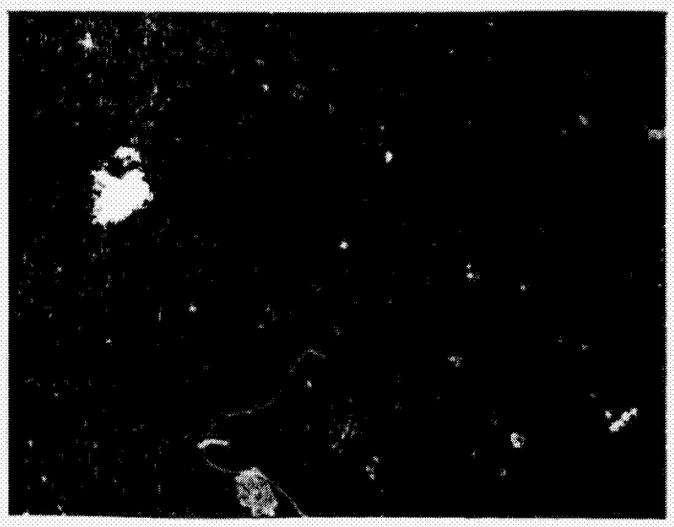

Figure 4.1

0.1 mm

Surface Crystallites of Splat-Cooled Sample

ORIGINAL PAGE IS
OF POOR QUALITY

Figure 4.2

Figure 4.3

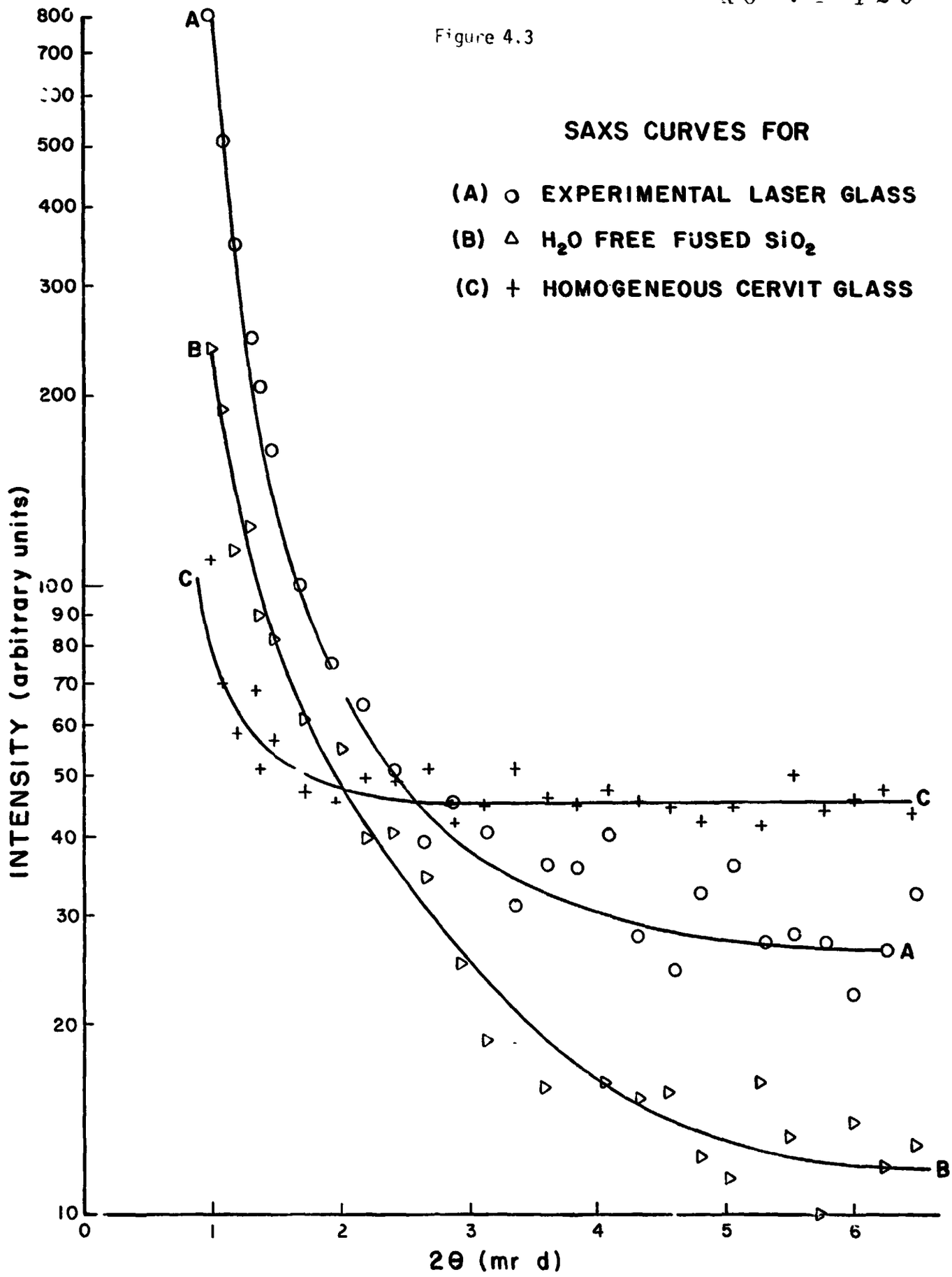
SAXS CURVES FOR
(A) ○ EXPERIMENTAL LASER GLASS
(B) △ H_2O FREE FUSED SiO_2
(C) + HOMOGENEOUS CERVIT GLASS
INTENSITY (arbitrary units)
2Θ (mr d)
A
B
C
800
700
500
400
300
200
100
90
80
70
60
50
40
30
20
10
0
1
2
3
4
5
6

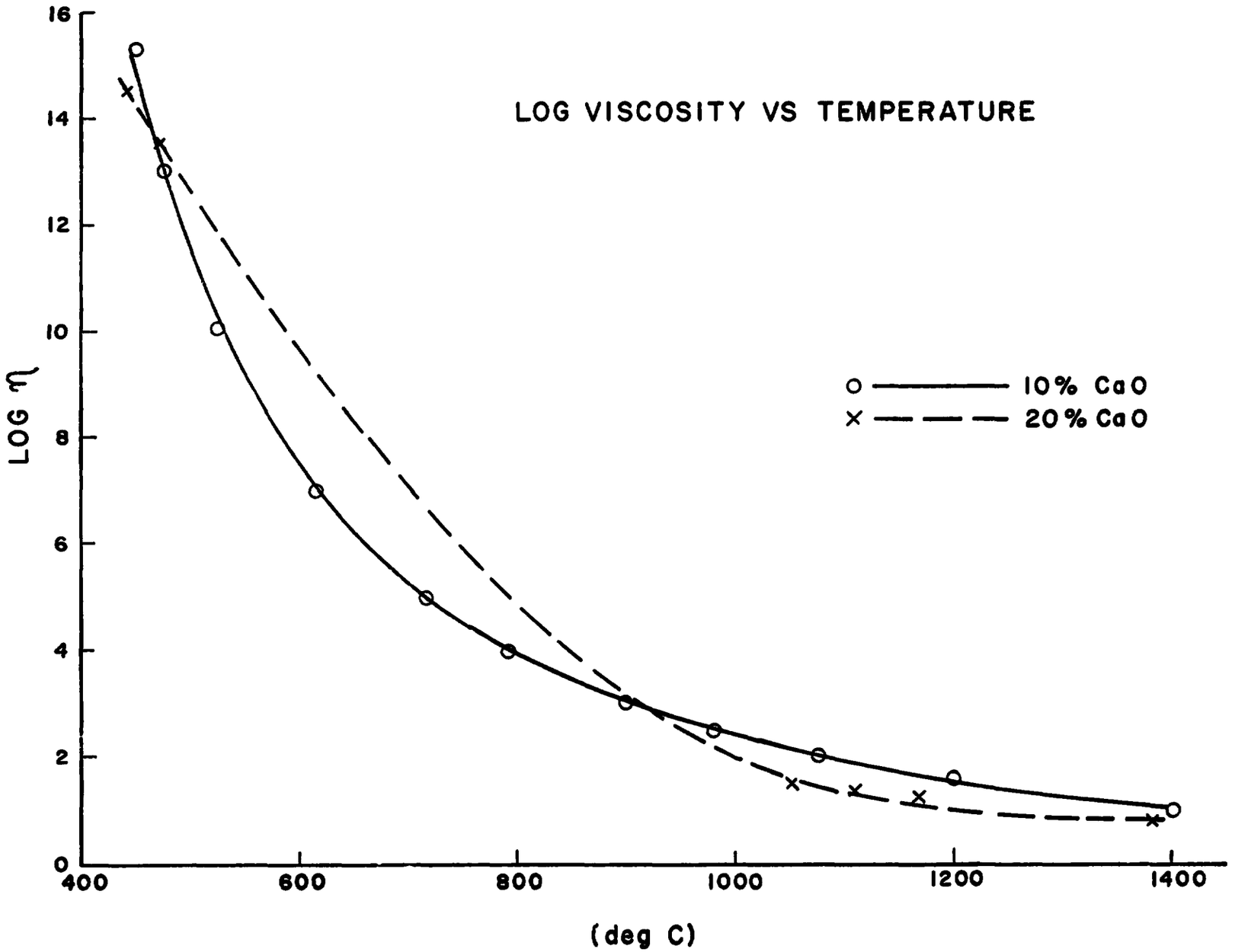
LOG VISCOSITY VS TEMPERATURE
LOG η
(deg C)
0
2
4
6
8
10
12
14
16
400
600
800
1000
1200
1400
10% CaO
20% CaO

Figure 5.1

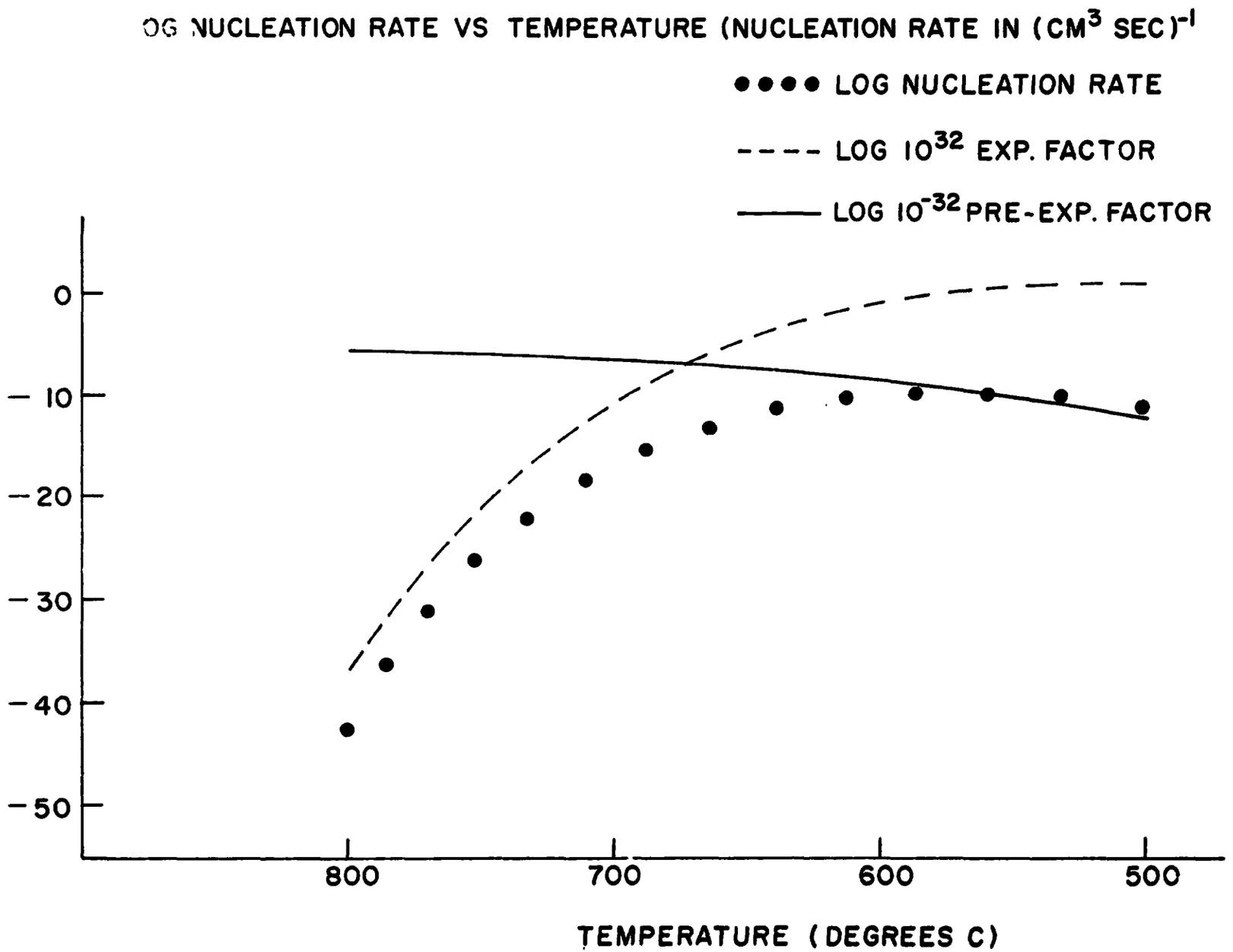
OG NUCLEATION RATE VS TEMPERATURE (NUCLEATION RATE IN (CM3 SEC)-1
LOG NUCLEATION RATE
LOG 10^32 EXP. FACTOR
LOG 10^-32 PRE-EXP. FACTOR
0
-10
-20
-30
-40
-50
800
700
600
500
TEMPERATURE (DEGREES C)

Figure 5.2

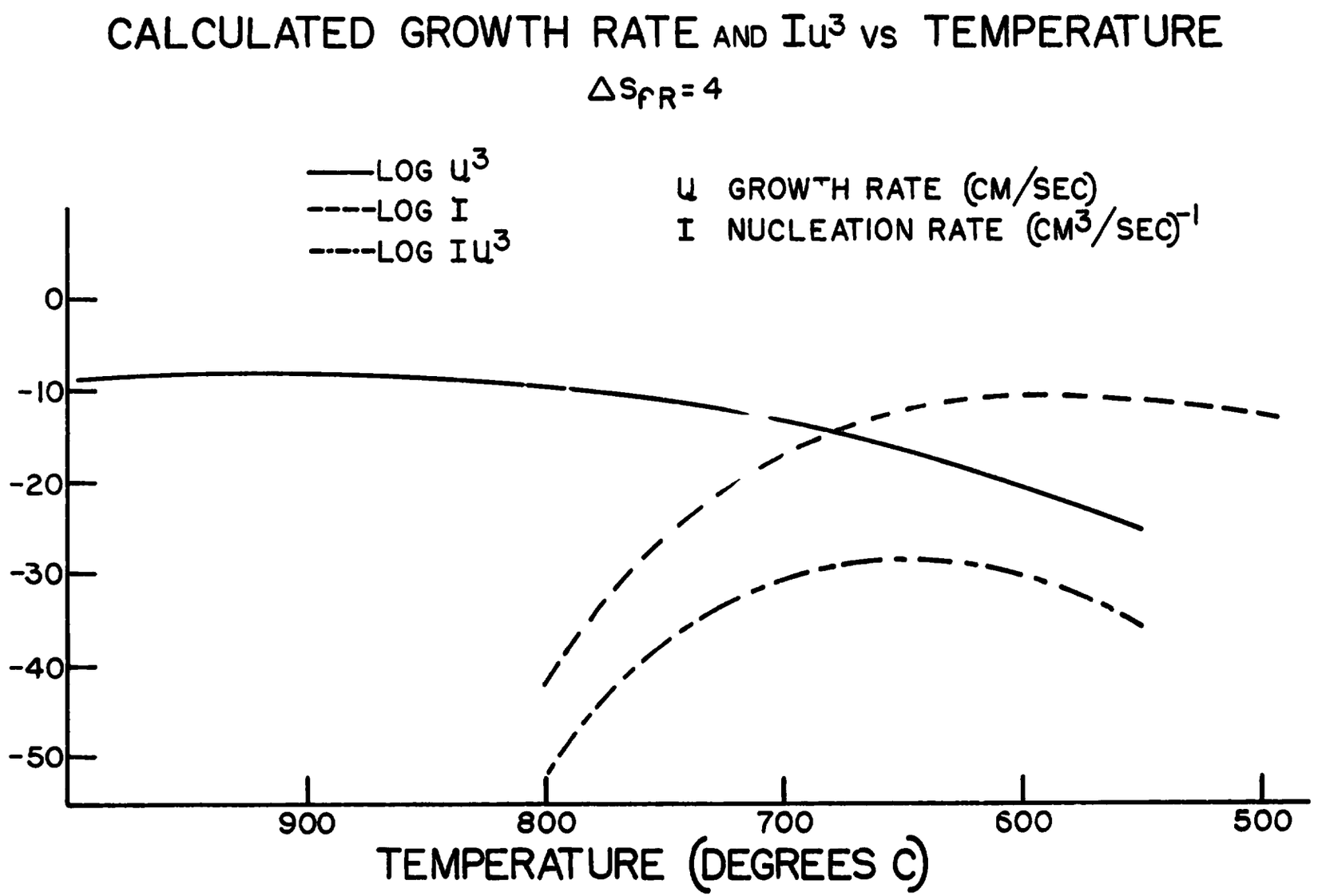
CALCULATED GROWTH RATE AND Iu3 vs TEMPERATURE
ΔSfR = 4
LOG u3
LOG I
LOG Iu3
u GROWTH RATE (CM/SEC)
I NUCLEATION RATE (CM3/SEC)-1
0
-10
-20
-30
-40
-50
900
800
700
600
500
TEMPERATURE (DEGREES C)

Figure 5.3

Figure 5.4

LOGARITHMS OF NUCLEATION AND GROWTHS RATES VS ΔS_{fR} AT T_{MAX}

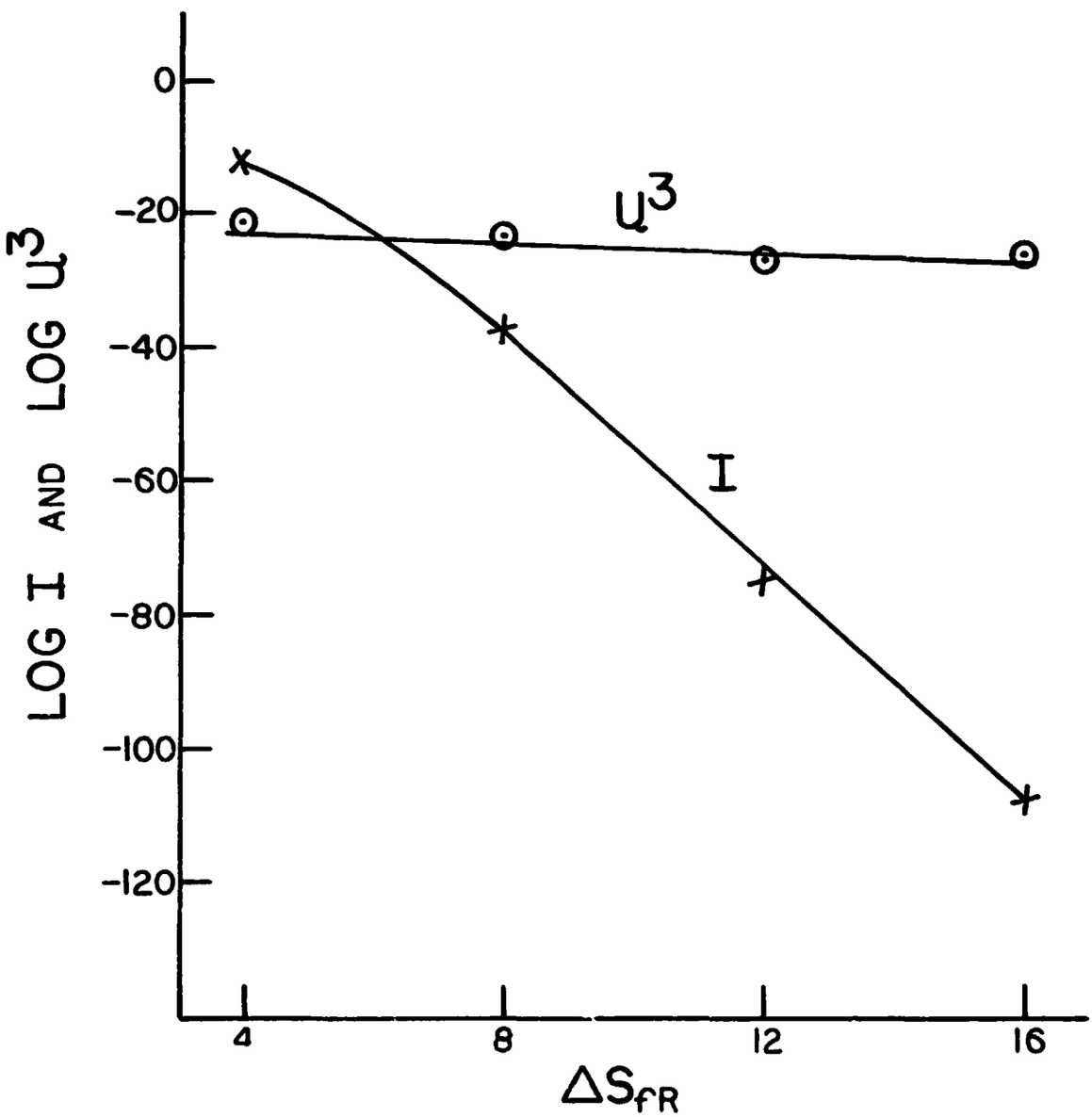

19

Figure 5.5

CRYSTALLIZATION FACTOR vs ΔS_{fR} AT T_{MAX}

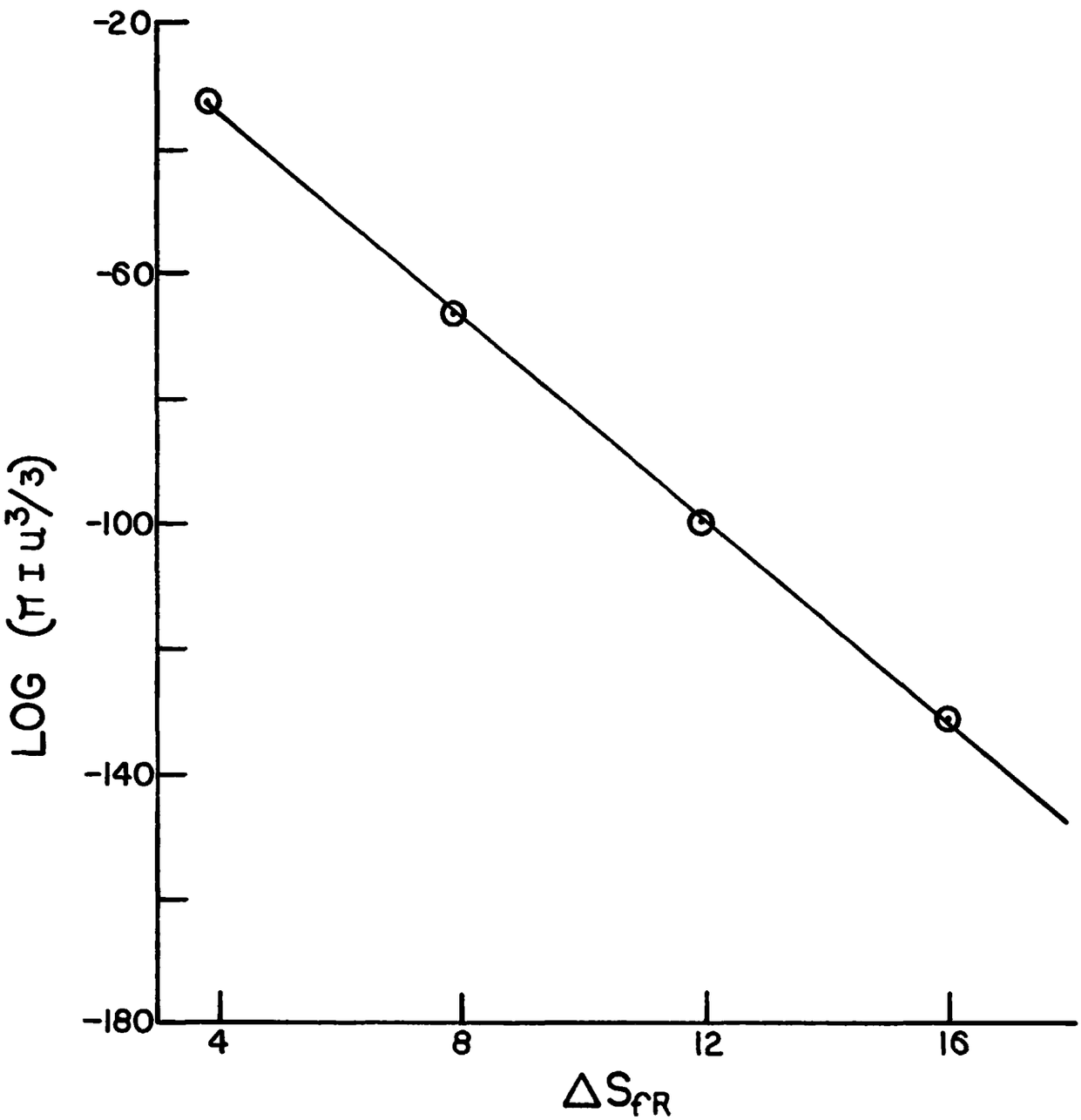

Figure 5.6

CRITICAL COOLING RATES vs X
FOR VARIOUS ΔS_{fR}

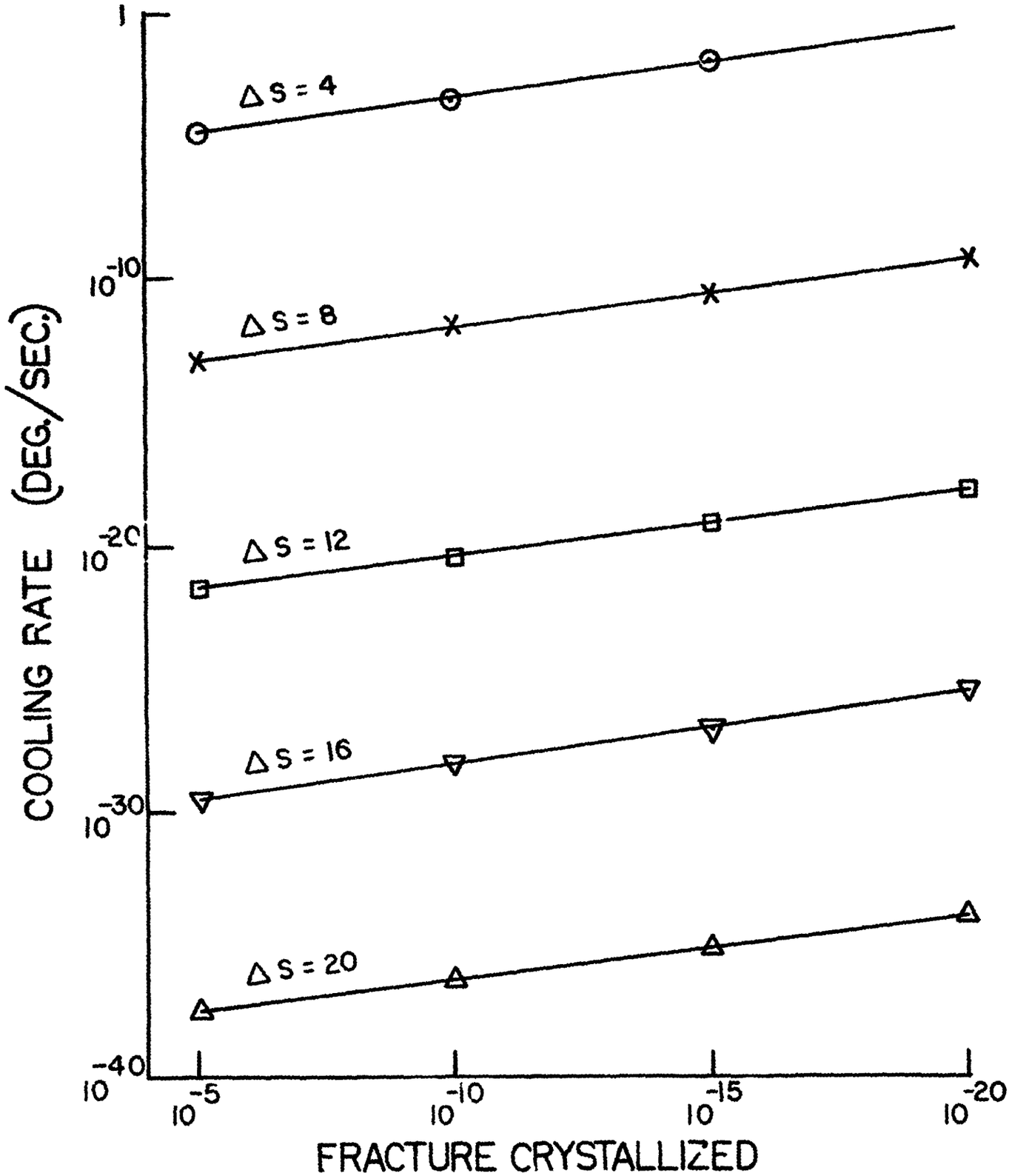

76